haematologica
Journal of the Ferrata Storti Foundation

Rapid recovery and functional resilience of bone marrow function post B-cell acute lymphoblastic leukemia

by Christina T. Jensen, Erik Hultin, Stefan Lang, Mina Mosaffa, Srivathsa Magadi, Johanna Tingvall-Gustafsson, David Bryder, Jan-Ingvar Jönsson, Shamit Soneji, Judit Svensson-Arvelund and Mikael Sigvardsson

Received: December 26, 2025.
Accepted: July 13, 2026.

Citation: Christina T Jensen, Erik Hultin, Stefan Lang, Mina Mosaffa, Srivathsa Magadi, Johanna Tingvall-Gustafsson, David Bryder, Jan-Ingvar Jönsson, Shamit Soneji, Judit Svensson-Arvelund and Mikael Sigvardsson. Rapid recovery and functional resilience of bone marrow function post B-cell acute lymphoblastic leukemia.
Haematologica. 2026 July 23. doi: 10.3324/haematol.2025.300439 [Epub ahead of print]

Rapid recovery and functional resilience of bone marrow function post B-cell acute lymphoblastic leukemia.

Christina T. Jensen[1#], Erik Hultin[2#], Stefan Lang[1], Mina Mosaffa[2], Srivathsa Magadi[2], Johanna Tingvall-Gustafsson[1,2], David Bryder[1], Jan-Ingvar Jönsson[2], Shamit Soneji[1], Judit Svensson-Arvelund[2] and Mikael Sigvardsson[1,2*]

[1]Division of Molecular Hematology, Lund Stem Cell Center, Lund University, Lund, Sweden

[2]Division of Molecular Medicine and Virology, Linköping University, Lab 1 level 13, 58135 Linköping, Sweden

[*] Corresponding author/Lead contact: mikael.sigvardsson@liu.se

# Indicates equal contributions

Author contributions: CTJ and EH in collaboration with MS designed the experiments. CTJ, EH and SM contributed to transplantation experiments. SS and SL performed sc-RNA seq analysis. JIJ and DB supervised transplantation and ELISA experiments. MM and JSA performed histological analysis. While CTJ, EH and MS wrote the first draft of the manuscript and generated the figures, all the authors contributed to the finalization of the manuscript.

Disclosures: None of the authors have anything to disclose related to the content of this paper.

Running title: Bone marrow resilience in B-lineage leukemia.

Data sharing: All data and reagents will be made available on request. ScRNA seq is deposited in GEO and details of scRNA seq data analysis is available at https://github.com/stela2502/BMResilience_ScRNAseq.

Acknowledgments: We are grateful to Helen Ekman, and Linda Bergstrand for technical assistance.

Funding resources: Swedish Cancer Society (23-3019P), the Swedish Childhood Cancer Foundation (2022-0019), Stiftelsen för Strategisk Forskning (SSF) (IB23-0001), the Swedish Research Council (2021-02379), and Linköping University.

Abstract

Leukemia often causes changes in the bone marrow (BM) microenvironment, but the extent to which this is associated with long term impairment of functional hematopoiesis remains unclear. Using a mouse model of B-cell acute lymphoblastic leukemia (B-ALL), we dissected how leukemia reshapes the BM microenvironment and redirects hematopoiesis to the spleen. We found that leukemic mice accumulate a markedly expanded pool of functional, long-term multilineage hematopoietic stem cells in the spleen, arising alongside a transient disruption of the CXCL12 gradient. Single-cell transcriptomics revealed changes in cytokine profiles, niche cell composition, and gene expression in the leukemic BM, while the changes in the spleen were less pronounced. Despite the niche distortion in the BM, selective ablation of leukemic cells led to rapid hematopoietic regeneration, with BM reconstitution detectable within just 4 days. Consistent with these findings, we observed an increased frequency of lineage restricted progenitor cells in B-ALL patients already 15 days after initiation of treatment. These findings uncover an unexpected robustness of BM niche function and suggest that B-ALL driven microenvironmental alterations do not prevent swift recovery of hematopoiesis following removal of malignant cells.

Introduction:

Many of the clinical manifestations of leukemia arise from progressive disruption of normal blood cell development (1). Although this could in part reflect direct displacement of normal progenitors from their natural niches (2), leukemia profoundly alters the bone marrow (BM) microenvironment (3-6), thereby promoting leukemia cell expansion (5, 7, 8) and compromising normal hematopoiesis (9-11). Chronic lymphoid leukemia (CLL) has been reported to target the self-renewal capacity of hematopoietic stem cells (HSCs) (12) while acute myeloid leukemia (AML) (11) and T-lineage acute lymphoid leukemia (T-ALL) (13), rather appear to target lineage restricted progenitor compartments. B-cell acute lymphoblastic leukemia (B-ALL) causes changes in vascularization (14), the composition and function of hematopoietic cells in the BM (15-17) as well as alterations in cytokine signaling and mesenchymal stromal-cell function (5, 10, 18, 19). Hematopoietic malignancies have been reported to cause a reduced expression of the Chemokine (C-X-C motif) ligand 12 (CXCL12), a critical regulator of HSC homing and retention in the BM (10, 20). Despite that *Cxcl12* is rather broadly expressed in the BM, lineage-specific inactivation of the coding gene demonstrated a critical role for endothelial- and Leptin receptor $(Lepr)^{+}$ stromal-derived CXCL12 in HSC niche formation (21). Reduced levels of chemokines such as CXCL12 could impair hematopoiesis due to defective HSC homing and contribute to the development of extramedullary hematopoiesis (EMH) (10, 20, 21), most commonly in the spleen but also in the liver, lymph nodes, and additional tissues (22). EMH is also observed in solid cancers including renal, prostate, colon, breast, lung, gastric and pancreatic malignancies, even in the absence of direct BM infiltration (22). This suggests that EMH is driven by systemic factors, such as inflammation, cytokine dysregulation or altered niche signaling, rather than by direct competition for BM niches. In addition to directly perturbing hematopoiesis, leukemia may

exploit EMH to generate blood cells that contribute to a more leukemia-permissive environment (23). Hence, defining the principles and consequences of EMH is essential for understanding host-tumor interactions.

To investigate B-ALL-induced EMH, we used a model based on primary leukemia cells from mice carrying combined heterozygous mutations in *Pax5* and *Ebf1* (24, 25). *PAX5* and *EBF1* encode two transcription factors that are frequently involved in the formation of leukemia in humans (26-29) and approximately 50% of the mice carrying these mutations develop spontaneous leukemia at about 30 weeks of age (24). Upon transplantation, these primary leukemia cells develop disease over 3-4 weeks without any need of conditioning (24), making this a reasonable model for investigations of leukemia impact on normal hematopoiesis. We show that splenic HSCs retain functional potential even in advanced disease, and that normal BM hematopoiesis rapidly recovers following leukemia cell removal despite profound microenvironmental alterations. Notably, this intrinsic resilience of BM function is also detected in patients with B-ALL as they display rapid restoration of hematopoietic progenitor cells following therapy.

Methods

Animal models and functional evaluation of progenitor cells.

Leukemia cells from CD45.2 mice carrying *Pax5*$^{+/-}$ and *Ebf1*$^{+/-}$ mutations (24) (*Pax5*$^{+/-}$*Ebf1*$^{+/-}$) were transferred to non-conditioned CD45.1 recipients via tail vein injection (150,000-200,000 cells per mouse).

TetO-Cas9 mice (Stock no: 029476 - B6.Cg-Col1a1<tm1(tetO-cas9)Sho>/J) crossed to R26m2rtTA mice to obtain a Doxycyclin (Dox) inducible (iCas9) mouse line. Cas9 inducible

tumor cells were then obtained by crossing the *Pax5*$^{+/-}$ *Ebf1*$^{+/-}$ mice with iCas9 mice (*Pax5*$^{+/-}$ *Ebf1*$^{+/-}$*iCAS9*$^{+}$). CRISPR guides to induce cell death were identified by searching for guides with a low specificity score in a repetitive area of the genome using Benchling (Biology Software. 2020). Chosen guides (sg292; GGAGCACTGTGACACCACAG and sg294; GGAGTACTGTGACACCACAG or sgR26 control; GCCGGTGCGCCGCCAATCAG) were cloned into pAW13.lentiGuide-emCherry plasmid (lentiguide-mCherry, Addgene plasmid # 104375) and pAW12.lentiGuide-eGFP plasmid (Addgene#: 104374, gifts from Richard Young). Viruses were prepared and used for transduction of *Pax5*$^{+/-}$*Ebf1*$^{+/-}$*iCAS9*$^{+}$ tumor cells. Transduced cells were sorted for expression of a vector encoded fluorescent markers and transplanted to CD45.1 hosts without conditioning. 14 days post transplantation, recipients were treated with Dox to induce Cas9 expression.

BM and spleen tissues from leukemic mice and PBS injected controls were harvested for fluorescence activated cell sorting (FACS, Table S1), immunofluorescent staining, enzyme-linked immunosorbent assay (ELISA), *in vitro* or *in vivo* functional analysis (Please see supplementary Materials) at the indicated timepoints after leukemia transplantation or administration of Dox. Procedures were performed with consent from the ethics committees at Lund- and Linköping Universities.

Sc-RNA Sequencing.

BM or spleen cells were isolated 16-19 days after leukemia transplantation. BM cells were sorted as positive for expression of stromal- or endothelial cell markers (CD31, CD34, CD44, CD51, CD106, CD114, CD140a, Sca1, or LEPR) and negative for hematopoietic markers (CD71, CD19, CD11b, B220, Ter119, and CD45). Spleen cells were sorted based on the absence of hematopoietic surface markers (Lin^{-} CD45.1^{-} CD45.2^{-} CD19^{-} CD71^{-}; please see

supplementary materials for details). Libraires were generated using the 10x Genomics Chromium platform and Single-cell Gene Expression (3´GEX, v3.1). Fastq files and gene count matrices were generated using *Cell Ranger* v4. Data was processed by *Scanpy* v1.10.1. Cells with >1,000 UMIs covering >100 genes were down-sampled to 1,000 UMIs per cell. The UMAPs are based on the 300 most variable genes. Details of the data analysis are available at: https://github.com/stela2502/BMResilience_ScRNAseq. The data is deposited in GEO (GSE316453).

Reanalysis of patient samples

BM from B-ALL patients (median age 6.5, 0-59 years) from diagnosis and 15-, 29- or 78-79-days post start of treatment (NOPHO2008 protocol (30)), was compared to data from healthy donors or lymphoma patients without BM engagement (31). The data were reanalyzed with consent from the Swedish National ethics board. UMAP for the visualization of FACS data associated with BM recovery was generated using FlowSOM clustering. B-ALL cells were identified as a $CD19^{+}$ cell clusters present only in leukemia samples. Flow cytometry data were analyzed and GraphPad Prism version 10.0.0.

Results

Leukemic spleen contains increased frequencies of functional HSCs.

To develop our understanding of B-ALL induced EMH, we transplanted primary *Pax5*$^{+/-}$ *Ebf1*$^{+/-}$ leukemia cells (CD45.2) (24) by tail vein injection into congenic (CD45.1) mice without conditioning (Figure 1A). Across recipient mice, FACS analysis revealed reduced BM cellularity (Figure S1A) associated with leukemia cell expansion (Figure S1B), while the spleens were enlarged containing roughly 35% leukemic cells 21 days after transplantation

(Figure 1B). Analysis of CD45.1^{+} hematopoietic progenitor frequency and absolute numbers revealed that leukemic spleens (TM) were enriched for multiple progenitor populations compared to PBS-injected controls (Figures 1C, S1C). These included total lineage-negative SCA1^{+}KIT^{+} (LSK) cells, CD150^{+} LSK (long-term hematopoietic stem cells), CD150$^{–}$ LSK (short-term multipotent progenitors), pro-granulocyte/monocyte progenitors (pGM), granulocyte/monocyte progenitors (GMP), pre-megakaryocyte/erythrocyte progenitors (pMegE), megakaryocyte progenitors (MkP), pre-colony-forming unit erythroid cells (pCFU-E), and colony-forming unit erythroid cells (CFU-E).

Determining the frequency and absolute numbers of CD45.1^{+} hematopoietic progenitors revealed that leukemic spleens (TM) contained higher frequencies as well as absolute numbers of total lineage negative SCA1^{+} KIT^{+} (LSK) cells, CD150^{+} LSK, including the long term stem cells, CD150^{-} LSK, including short term multipotent progenitors, pro-granulocyte/monocyte progenitors (pGM), granulocyte/monocyte progenitors (GMP), pre-megakaryocyte/erythrocyte progenitor (pMegE), megakaryocyte progenitors (MkP), pre-colony forming unit erythroid cells (pCFU-E) and colony forming erythroid (CFU-E) cells as compared to spleen from PBS injected control animals (Figure 1C, S1C for gating scheme).

To obtain a high resolution analysis of the LSK compartment, we combined CD150 with CD48 (32) and EPCR/CD201 (33) (Figure 1D). This analysis revealed that the leukemic BM LSK compartment contained a higher fraction of phenotypic long term (LT)-HSCs (CD150^{+} CD48^{-} CD201^{+}), and Multipotent progenitor (MPP) 2 cells (CD150^{+} CD48^{+}) and a lower frequency of Lymphoid primed multipotent progenitor (LMPP) 3/4 cells (CD150^{-} CD48^{+}) as compared to control BM (Figure 1E). The composition of the splenic LSK compartment was comparable

to what we observed in the BM. Thus, the increased frequency of progenitor cells in leukemic spleen was not linked to major changes in cellular composition (Figure 1E).

While the frequency of hematopoietic progenitors in normal spleen was too low for extensive high resolution functional analysis, we did obtain enough cells to perform single cell *in vitro* cloning assays. Single LT-HSCs, ST-HSCs as well as MPP2-4 were sorted into Myelocult M3434 media and the cloning frequency was determined using light microscopy 10 days after seeding (Figure 2A). While LT-HSCs and MPPs from control spleen generated a lower frequency of clones (Figure 2B), all the populations from leukemic spleen were functionally comparable to that observed in progenitors from BM. To investigate the functionality of these cells, we analyzed 5 of the clones from each mouse and population by FACS. Most of the clones contained $CD45^+$ $CD11b^+$ $CD16/32^+$ $Ly6c^+$ monocytes, in some cases in combination with $CD45^{low/neg}$ $CD71^+$ erythroid progenitors. We did not detect any significant differences in cellular output among the populations (Figure S1D). To further investigate multipotency in the progenitors, we made bulk cultures of $CD150^+$ LSK cells (32) from control BM and leukemic BM and spleen in Myelocult M3434 media. All three populations generated erythroid (BFU-E), granulocyte/monocyte colonies (CFU-G and CFU-M) and colonies composed of multiple cell types (CFU-GM and CFU-GEMM) at similar frequency (Figure S1E). These data suggest that the phenotypic progenitors in the leukemic spleen have a superior cloning capacity as compared to those in a healthy spleen, making them functionally comparable to the cells found in mouse BM.

To evaluate the *in vivo* potential of phenotypic LT-HSCs in BM and leukemic spleen, we transplanted equal numbers of $CD150^+$ $CD48^-$ $CD201^+$ LSK cells from control BM (BM PBS), leukemic BM (BM TM), or leukemic spleen (SPL TM) into lethally irradiated CD45.2 mice

and tracked donor-derived hematopoiesis for 24 weeks. Even though we did not detect any significant differences in overall output of CD45.1$^+$ cells, leukemia exposed BM HSCs displayed a reduced myeloid (Gr1/Mac1$^+$) reconstitution capacity as compared to HSCs from the BM of control mice or leukemic spleen (Figure 2C). The functional impairment of leukemia-exposed BM LT-HSCs was also reflected in reduced numbers and frequencies of donor derived lineage-restricted progenitors in the BM 26 weeks after transplantation (Figure 2D). These data suggest that the phenotypic LT-HSCs detected in the spleen of leukemic mice represent bona fide HSCs with long-term reconstitution capacity.

Hematopoietic progenitors occupy a perivascular niche in the leukemic spleen.

It has been reported that HSCs in the spleen reside in a perisinusoidal niche in the red pulp (34). To determine if B-ALL-induced EMH results in alterations in the splenic HCS niche, we performed single cell RNA-seq (scRNA-seq) from control and leukemic spleen. As we were unable to identify classical stromal cell populations using flow cytometry, we sorted Lin$^-$ (CD45, B220, Ter119, CD11b, CD11c, NK1.1, CD3) CD45.1$^-$ CD45.2$^-$ CD19$^-$ CD71$^-$ cells for scRNA-seq. Projecting the analysis of 1502 control, and 2309 cells from the leukemic spleen in uniform manifold approximation and projection (UMAP) (Figure 3A, S2A-B), we identified 16 Leiden clusters. Applying Single R to annotate the defined clusters revealed that the leukemic spleen was dominated by endothelial cells (Figure S2C). To increase the resolution of the cell labelling, we generated heatmaps based on the expression of genes reported to define specific subpopulations of nonhematopoietic BM cells (35) (Figure 3B). To reduce the impact of the differences in cluster size, we based expression values on the ten centrally ranked cells within each cluster. We detected *Kitl* expression in combination with endothelial markers such as *Kdr*, *Eng* and *Thbd* (35) in cluster 0, 1, 3, 4, 6 and 7 (Figure 3B, S2D), supporting the idea that splenic endothelial cells are a major source of *Kitl* in the spleen (36). Analysis of

endothelial marker gene expression (37) revealed the presence of general markers, including *Flt1* and *Tie1*, as well as *Ptprb* and *Cd93*, which are more selectively expressed in capillary endothelial cells (Figure S2E). The expression of *Cxcl12* was largely restricted to cluster 6 composed of cells expressing the arterial markers *Mecom* and *Dll4* (Figure S2D, E) (37). These cells also expressed *Lepr* (Figure 3B), a marker for HSC supporting *Kitl* and *Cxcl12* expressing perivascular stromal cells in the spleen (21, 34). Hence, even though the relative contribution of cells to defined clusters varied, we did not detect major shifts in molecular signatures of putative niche cells in normal as compared to leukemic spleen.

To determine the microanatomical location of HSCs in the leukemic spleen, we performed histological analysis of sections generated form control and leukemic mice. Staining with anti-CD45.2 suggested that the B-ALL cells were primarily localized to the white pulp (Figure S3A). To localize HSCs, we stained tissue sections with antibodies against the stem and progenitor markers CD48 and EPCR/CD201, as well as the endothelial marker CD31 (Figure 4A). Even though this marker combination does not allow for a high-resolution analysis, it allows us to distinguish the MPP from the HSC compartment (32, 33). While we detected an increased abundance of $EPCR^+$ $CD48^-$ HSCs (Figure 4B), these cells resided in the red pulp of both leukemic and control spleen (Figure 4A). We did not detect any changes in the density of endothelial cells (Figure S3B) or the distance between $EPCR^+$ cells and the nearest $CD31^+$ cell (Figure 4C). Hence, even though we detected signs of environmental adaptation in the leukemic spleen, the hematopoietic niche appears to be rather preserved even in advanced leukemia and EMH.

Leukemia progression involves a change in CXCL12 gradients.

It has been proposed that leukemia causes disruptions of the BM microenvironment possibly contributing to EMH (10, 18, 19). To investigate the impact of B-ALL on the BM microenvironment, we conducted scRNA-seq on non-hematopoietic BM cells from normal and leukemic mice. To enrich for non-hematopoietic cells, we sorted cells expressing at least one of the markers CD31, CD34, CD44, CD51, CD106, CD114, CD140a, SCA1, or LEPR, and lacking CD71, CD19, CD11b, B220, Ter119, and CD45. Plotting the data generated from 6401 cells from the control and 1750 cells from leukemic BM in a UMAP (Figure 5A) identified 23 Leiden clusters (Figure 5A, S4A-B) and SingleR-based cell annotation (Figure S4C) indicated that several clusters dominated by cells from control BM (Figure S4A) corresponded to hematopoietic lineages, most notably basophils, reported to express low levels of CD45 (38). Five clusters (7, 8, 17, 18 and 20) were classified as fibroblasts and clusters 5 and 15 were suggested to represent endothelial cells. Clusters 5 and 15 expressed *Emcn*, *Kdr* and *Eng*, confirming their annotation as endothelial cells, while cluster 17 was composed of cells expressing *Ly6a*, *Vim* and *Fn1*, consistent with a fibroblast identity (35) (Figure 5B). Expression of *Spp1*, *Alpl* and *Fap2* defined cluster 18 as osteoblasts, and *Kitl*, *Vcam1* and *Lepr* expression in cluster 7, 8, 20 and 22, identify them as stromal cells. Notably, stromal cell cluster 7 was composed almost exclusively of cells from the control, while the stromal cells in cluster 8 were uniquely detected in leukemic mice (Figure 5A, S4A). Furthermore, cells from leukemic BM contributed to a higher degree than control cells to the endothelial cell clusters 5 and 15. These endothelial cells express *Cd93* and *Ptprb*, which are selectively enriched in capillary endothelium, as well as arterial markers such as *Mecom* and *Dll4* (37) (Figure S4D). These data support that B-ALL induce alterations in cellular composition as well as molecular features of niche cells in the BM.

It has been reported that B-ALL reduces the overall expression of *Cxcl12* in the BM (10, 18, 19), increasing the migration of HSCs from the BM. To investigate how B-ALL impacts the production of cytokines in the BM, we determined the expression of a set of cytokines in our scRNA-seq data (Figure 6A). While the endothelial cells in the BM (Clusters 5 and 15) produced *Cxcl12* and *KitL* mRNA, the stromal cells in clusters 7 and 8 expressed the highest levels of message for most of the selected chemokines (Figure 6A). Cluster 8, generated from B-ALL exposed stromal cells, expressed lower levels of *Cxcl12*, *Bmp4* and *Fgf7* while expressing higher levels of *Ccl19* message than stroma cells from control BM. Although the scRNA-seq data suggested that *Cxcl12* expression is lower in stromal cells from leukemic BM (Figure 6A, S4E), the extensive changes in cellular composition as well as CXCR4 expression on the tumor cells (39), makes it difficult to determine the total levels of accessible CXCL12 in the BM or spleen. To estimate the relative levels of available CXCL12, we used cell free supernatants generated from control as well as leukemic BM and spleen for ELISA. Six days after transplantation, leukemic cells were undetectable in both BM and spleen (Figure 6B) and the CXCL12 levels were not significantly different from that of controls (Figure 6C). By day 10, leukemic cells comprised approximately 50% of the BM cells and ≈5% of the spleen cells (Figure 6B). At this time CXCL12 levels were drastically reduced in supernatants from leukemic BM, while the levels in the spleen were more modestly decreased (Figure 6C). As the levels of free CXCL12 in the spleen is reduced in terminally sick mice (Figure S4F), this gradient shift is likely to be transient. Concomitant with these changes, we observed more LSK cells in the spleen and fewer in the BM (Figure 6D). These data suggest that leukemia progression induces a transient alteration of CXCL12 gradients possibly promoting the redistribution of hematopoietic progenitors from the BM to the spleen.

BM functionality is rapidly restored upon elimination of leukemia cells.

As B-ALL has been shown to disrupt the BM microenvironment and cause displacement of HSCs (10), we wanted to determine the ability of the BM to functionally recover upon elimination of leukemic cells. To this end, we crossed *Ebf1*$^{+/-}$*Pax5*$^{+/-}$ mice to animals carrying a Doxycycline (Dox) inducible CAS9. These mice developed leukemia at around 30 weeks of age, generating *Ebf1*$^{+/-}$*Pax5*$^{+/-}$ B-ALLs with an inducible CAS9 coding gene. To selectively eliminate the leukemia cells, we transduced them with guide RNAs (gRNAs) targeting repetitive genomic sequences ("Kill switch (KS) guides"), so that Dox administration in leukemic mice would cause DNA damage and thereby selectively ablate the transformed cells (Figure 7A). To avoid the CAS9 protein to be recognized as a neoantigen in the leukemic mice, we transplanted CD45.2^{+} leukemia cells to CD45.1^{+}TetR^{+}iCAS9 mice. Before administration of Dox, the leukemia cells colonized the BM and spleen with between 80- and 90% leukemic cells in the BM two weeks after transplantation (Figure 7B). Animals transplanted with leukemia cells expressing a control guide targeting the Rosa 26 (R26) locus reached the humane end point 2-3 days after initiation of treatment and were euthanized. In mice transplanted with KS-guide–expressing cells, administration of Dox resulted in a dramatic reduction of leukemia burden in both BM and spleen as early as four days after initiation of treatment (Figure 7B). The reduction in leukemia burden resulted in a rapid reestablishment of hematopoiesis in the BM with significant increase of both CD150^{+} and CD150^{-} LSK cells already 4 days after administration of Dox (Figure 7C upper panel). Eight days after initiation of treatment, myelopoiesis was robustly re-established as we detected both monocyte/granulocyte progenitors (pGM and GMP), erythroid progenitor populations (pCFU-E and CFU-E) and megakaryocyte progenitors (pMegE and MkP) (Figure 7C lower panel). 14 days after the initiation of treatment, the numbers of progenitor cells were comparable to those in control mice. Thus, although B-ALL induces major alterations in the BM microenvironment, these changes do not cause lasting impairment of the marrow's ability to generate blood cells

once the leukemic burden is reduced. The decline in leukemia load was also accompanied by a decrease in spleen size (Figure S5A-B). However, we still detected increased frequency of $CD150^+$ LSK cells, in the spleen 14 days after initiation of Dox administration (Figure 7D).

To investigate hematopoietic recovery in B-ALL patients following therapy, we analyzed FACS data from sequential BM samples collected as part of routine diagnostics from patients treated according to the NOPHO2008 protocol (31). Samples were stained for expression of CD66c, CD58, CD20, CD38, CD19, CD123, CD34, CD10, CD22 and CD45. We initially generated a UMAP embedding based on all surface markers (Figure 8A, S5C) and performed high-resolution cell-type annotation using FlowSOM. Hematopoietic progenitor cells were identified as $CD45^+$ $CD34^+$ and negative for CD19, CD22, CD20 and CD66c. These cells were further subdivided into early and late progenitors based on CD38 expression, which marks lineage restricted progenitors but is low or absent on HSCs (40). Leukemic cells were identified by comparing UMAP projections of $CD19^+$ cells from patients to those from normal controls (Figure 8A). The fraction of leukemic cells was reduced already 15 days after initiation of treatment (Figure 8B). Although our use of clinical diagnostic material precluded direct comparisons of absolute cell numbers, we did detect an increase in the frequency of $CD38^+$ progenitor cells, consistent with enhanced production of lineage restricted progenitor cells - a population preferentially targeted in B-ALL (17). Notably, while a largely normal BM cell composition was not restored until 78-79 days after treatment (Figure 8C), these findings indicate early recovery of BM hematopoietic output already within the first 15 days of therapy.

Discussion

Our results show that, despite B-ALL-induced alterations in the BM microenvironment and displacement of hematopoietic progenitors, efficient removal of leukemic cells leads to a rapid

re-establishment of functional hematopoiesis. The impact of leukemia on the BM has been extensively studied, revealing roles for non-hematopoietic cells in both the impairment of normal blood cell production (9-11) and the establishment of a tumor-permissive environment (5, 7, 8, 41). Microenvironmental alterations may also underlie the EMH observed in malignant disease (22), and our data are consistent with previous observations showing reduced CXCL12 protein levels in the BM in B-ALL (10, 18, 19). This reduction was most prominent in LeptinR^{+} stromal cells, which is noteworthy in light of that selective inactivation of *Cxcl12* in these cells results in increased accumulation of HSCs in the spleen (21). Although we detected reduced expression of *Cxcl12* within the stromal cell compartment, this downregulation was modest as compared to the dramatic reduction in free CXCL12 protein in the BM (Figure 6C). Together, these data suggest that leukemia cells may compete with normal progenitor cells for available CXCL12, thereby contributing to EMH through transient and sequential shifts in chemokine gradients.

The BM niche is highly complex, and it has been estimated that over 20 cell types contribute to the regulation of hematopoiesis (42). These include osteoblastic cells (43), *Cxcl12* expressing stromal cells (44) and endothelial cells (32). BM endothelial cells can be subdivided into *Sca1* (*Ly6a*)$^{+}$ arterial and *Sca1*$^{-}$ sinusoidal cells (45). While sinusoidal cells are considered as the normal path for the exit of blood cells to the periphery, regions of arteriolar cells have been suggested to be the main site for HSCs (46). Our scRNA-seq analysis suggests that the BM contains a substantial *Ly6a*$^{-}$expressing endothelial population that does not display major changes in transcriptional profile in response to leukemia (Figure 5 Cluster 5). Increased vessel formation in AML has been reported to result in vascular leakiness and hypoxia within the BM (47) indicating changes in the BM micro-anatomy. Our analysis does not allow us to determine if the rapid recovery of hematopoiesis in the BM upon depletion of leukemia cells, is a result

of reestablishment of a normal niche structure. However, in contrast to the stromal cell compartment, endothelial cells retained rather normal molecular characteristic (Figure 5A). Preservation of the vascular niche may therefore partially explain the rapid recovery of hematopoiesis observed following removal of leukemic cells (Figure 7C).

It has been reported that splenic HSCs localize to a perisinusoidal niche within the red pulp in healthy mice (34). The vascular niche would also appear to be the most prominent niche in the leukemic spleen as the majority of the $CD48^{-}EPCR^{+}$ cells were detected in the red pulp within a Euclidian distance of 30 micrometers from the closest $CD31^{+}$ cell (Figure 3F). Furthermore, we identified a *Ly6a*-expressing arteriolar compartment expressing *Cxcl12* as well as *KitL* in the spleen of both control and leukemic mice, supporting the notion that splenic HSCs reside in a vascular niche. Although the spleen has been reported to harbor a *KitL*- and *Cxcl12*-expressing perivascular stromal cell compartment (34), we did not detect substantial expression of these genes outside the endothelial compartments in either controls or leukemic mice, suggesting that the splenic microenvironmental undergoes subtle adaptation in response to leukemia.

While our findings support the idea that leukemia induces substantial changes in the BM microenvironment, they suggest that the BM possesses an inherent resilience following depletion of leukemia cells. This could be explained by the presence of functional HSCs in the leukemic BM in both mouse models and B-ALL patients (17). The capacity of the splenic niche to support HSC function is supported by previous findings showing that, although BM- and spleen-derived HSCs display somewhat different cell-cycle dynamics, they are largely functionally similar under steady-state conditions (48). Consistent with this, our data show that phenotypic HSCs in B-ALL-infiltrated spleen retain functional capacity, including homing to

the BM (Figure 2D). While the frequency of HSCs in the spleen remains relatively constant after depletion of leukemia cells (Figure 7D), the rapid reduction in total splenic cell numbers (Figure S5A) suggests a decrease in the absolute number of splenic HSCs. Together, these findings indicate that the splenic niche may function as a reservoir for functional HSCs in B-ALL.

Our analysis of FACS data from B-ALL patients indicates that hematopoiesis can be rapidly restored, even in individuals receiving chemotherapy, (vincristine, doxorubicin, glucocorticoids and intrathecal methotrexate), expected to impair normal blood formation (30). Although the specific features of a given leukemia undoubtedly shape its impact on the BM microenvironment, leukocyte recovery after chemotherapy has been identified as an independent prognostic factor in both AML and ALL (49), linking restoration of hematopoiesis to clinical outcome. We believe our data highlights an inherent resilience of the BM that may be exploited in future strategies for management of leukemic disease.

References:

1. Hunger SP, Mullighan CG. Acute lymphoblastic leukemia in children. N Engl J Med. 2015;373(16):1541-1552.

2. van Bekkum DW, Prins ME, Hagenbeek A. The mechanism of inhibition of haemopoiesis in acute leukaemia. Blood Cells. 1981;7(1):91-103.

3. Hoggatt J, Kfoury Y, Scadden DT. Hematopoietic stem cell niche in health and disease. Annu Rev Pathol. 2016;11:555-581.

4. Boulais PE, Frenette PS. Making sense of hematopoietic stem cell niches. Blood. 2015;125(17):2621-2629.

5. Ahsberg J, Xiao P, Okuyama K, et al. Progression of progenitor B cell leukemia is associated with alterations of the bone marrow micro-environment. Haematologica. 2020;105(3):e102-e106.

6. von der Heide EK, Neumann M, Vosberg S, et al. Molecular alterations in bone marrow mesenchymal stromal cells derived from acute myeloid leukemia patients. Leukemia. 2017;31(5):1069-1078.

7. Kumar B, Garcia M, Weng L, et al. Acute myeloid leukemia transforms the bone marrow niche into a leukemia-permissive microenvironment through exosome secretion. Leukemia. 2018;32(3):575-587.

8. Shafat MS, Oellerich T, Mohr S, et al. Leukemic blasts program bone marrow adipocytes to generate a protumoral microenvironment. Blood. 2017;129(10):1320-1332.

9. Boyd AL, Reid JC, Salci KR, et al. Acute myeloid leukaemia disrupts endogenous myelo-erythropoiesis by compromising the adipocyte bone marrow niche. Nat Cell Biol. 2017;19(11):1336-1347.

10. Colmone A, Amorim M, Pontier AL, Wang S, Jablonski E, Sipkins DA. Leukemic cells create bone marrow niches that disrupt the behavior of normal hematopoietic progenitor cells. Science. 2008;322(5909):1861-1865.

11. Miraki-Moud F, Anjos-Afonso F, Hodby KA, et al. Acute myeloid leukemia does not deplete normal hematopoietic stem cells but induces cytopenias by impeding their differentiation. Proc Natl Acad Sci U S A. 2013;110(33):13576-13581.

12. Kikushige Y, Ishikawa F, Miyamoto T, et al. Self-renewing hematopoietic stem cell is the primary target in pathogenesis of human chronic lymphocytic leukemia. Cancer Cell. 2011;20(2):246-259.

13. Hu X, Shen H, Tian C, et al. Kinetics of normal hematopoietic stem and progenitor cells in a Notch1-induced leukemia model. Blood. 2009;114(18):3783-3792.

14. Perez-Atayde AR, Sallan SE, Tedrow U, Connors S, Allred E, Folkman J. Spectrum of tumor angiogenesis in the bone marrow of children with acute lymphoblastic leukemia. Am J Pathol. 1997;150(3):815-821.

15. Witkowski MT, Dolgalev I, Evensen NA, et al. Extensive remodeling of the immune microenvironment in B cell acute lymphoblastic leukemia. Cancer Cell. 2020;37(6):867-882.

16. Vilchis-Ordonez A, Contreras-Quiroz A, Vadillo E, et al. Bone marrow cells in acute lymphoblastic leukemia create a proinflammatory microenvironment influencing normal hematopoietic differentiation fates. Biomed Res Int. 2015;2015:386165.

17. Jensen CT, Ahsberg J, Tingvall-Gustafsson J, et al. B-lineage acute lymphoblastic leukemia causes cell autonomous defects in long-term hematopoietic stem cell function. Haematologica. 2023;108(11):3175-3180.

18. Balandran JC, Purizaca J, Enciso J, et al. Pro-inflammatory-related loss of CXCL12 niche promotes acute lymphoblastic leukemic progression at the expense of normal lymphopoiesis. Front Immunol. 2016;7:666.

19. van den Berk LC, van der Veer A, Willemse ME, et al. Disturbed CXCR4/CXCL12 axis in paediatric precursor B-cell acute lymphoblastic leukaemia. Br J Haematol. 2014;166(2):240-249.

20. Zhang B, Ho YW, Huang Q, et al. Altered microenvironmental regulation of leukemic and normal stem cells in chronic myelogenous leukemia. Cancer Cell. 2012;21(4):577-592.

21. Ding L, Morrison SJ. Haematopoietic stem cells and early lymphoid progenitors occupy distinct bone marrow niches. Nature. 2013;495(7440):231-235.

22. Barisas DAG, Choi K. Extramedullary hematopoiesis in cancer. Exp Mol Med. 2024;56(3):549-558.

23. Cortez-Retamozo V, Etzrodt M, Newton A, et al. Origins of tumor-associated macrophages and neutrophils. Proc Natl Acad Sci U S A. 2012;109(7):2491-2496.

24. Prasad MA, Ungerback J, Ahsberg J, et al. Ebf1 heterozygosity results in increased DNA damage in pro-B cells and their synergistic transformation by Pax5 haploinsufficiency. Blood. 2015;125(26):4052-4059.

25. Somasundaram R, Ahsberg J, Okuyama K, et al. Clonal conversion of B lymphoid leukemia reveals cross-lineage transfer of malignant states. Genes Dev. 2016;30(22):2486-2499.

26. Mullighan CG, Goorha S, Radtke I, et al. Genome-wide analysis of genetic alterations in acute lymphoblastic leukaemia. Nature. 2007;446(7137):758-764.

27. Mullighan CG, Miller CB, Radtke I, et al. BCR-ABL1 lymphoblastic leukaemia is characterized by the deletion of Ikaros. Nature. 2008;453(7191):110-114.

28. Kuiper RP, Schoenmakers EF, van Reijmersdal SV, et al. High-resolution genomic profiling of childhood ALL reveals novel recurrent genetic lesions affecting pathways involved in lymphocyte differentiation and cell cycle progression. Leukemia. 2007;21(6):1258-1266.

29. Somasundaram R, Prasad MA, Ungerback J, Sigvardsson M. Transcription factor networks in B-cell differentiation link development to acute lymphoid leukemia. Blood. 2015;126(2):144-152.

30. Toft N, Birgens H, Abrahamsson J, et al. Results of NOPHO ALL2008 treatment for patients aged 1-45 years with acute lymphoblastic leukemia. Leukemia. 2018;32(3):606-615.

31. Modvig S, Hallbook H, Madsen HO, et al. Value of flow cytometry for MRD-based relapse prediction in B-cell precursor ALL in a multicenter setting. Leukemia. 2021;35(7):1894-1906.

32. Kiel MJ, Yilmaz OH, Iwashita T, Yilmaz OH, Terhorst C, Morrison SJ. SLAM family receptors distinguish hematopoietic stem and progenitor cells and reveal endothelial niches for stem cells. Cell. 2005;121(7):1109-1121.

33. Balazs AB, Fabian AJ, Esmon CT, Mulligan RC. Endothelial protein C receptor (CD201) explicitly identifies hematopoietic stem cells in murine bone marrow. Blood. 2006;107(6):2317-2321.

34. Inra CN, Zhou BO, Acar M, et al. A perisinusoidal niche for extramedullary haematopoiesis in the spleen. Nature. 2015;527(7579):466-471.

35. Baryawno N, Przybylski D, Kowalczyk MS, et al. A cellular taxonomy of the bone marrow stroma in homeostasis and leukemia. Cell. 2019;177(7):1915-1932.

36. Ding L, Saunders TL, Enikolopov G, Morrison SJ. Endothelial and perivascular cells maintain haematopoietic stem cells. Nature. 2012;481(7382):457-462.

37. Trimm E, Red-Horse K. Vascular endothelial cell development and diversity. Nat Rev Cardiol. 2023;20(3):197-210.

38. Tchen J, Simon Q, Chapart L, et al. CT-M8 Mice: a new mouse model demonstrates that basophils have a nonredundant role in lupus-like disease development. Front Immunol. 2022;13:900532.

39. Mohle R, Schittenhelm M, Failenschmid C, et al. Functional response of leukaemic blasts to stromal cell-derived factor-1 correlates with preferential expression of the chemokine receptor CXCR4 in acute myelomonocytic and lymphoblastic leukaemia. Br J Haematol. 2000;110(3):563-572.

40. Notta F, Zandi S, Takayama N, et al. Distinct routes of lineage development reshape the human blood hierarchy across ontogeny. Science. 2016;351(6269):aab2116.

41. Schepers K, Pietras EM, Reynaud D, et al. Myeloproliferative neoplasia remodels the endosteal bone marrow niche into a self-reinforcing leukemic niche. Cell Stem Cell. 2013;13(3):285-299.

42. Pinho S, Frenette PS. Haematopoietic stem cell activity and interactions with the niche. Nat Rev Mol Cell Biol. 2019;20(5):303-320.

43. Calvi LM, Adams GB, Weibrecht KW, et al. Osteoblastic cells regulate the haematopoietic stem cell niche. Nature. 2003;425(6960):841-846.

44. Mendez-Ferrer S, Michurina TV, Ferraro F, et al. Mesenchymal and haematopoietic stem cells form a unique bone marrow niche. Nature. 2010;466(7308):829-834.

45. Hooper AT, Butler JM, Nolan DJ, et al. Engraftment and reconstitution of hematopoiesis is dependent on VEGFR2-mediated regeneration of sinusoidal endothelial cells. Cell Stem Cell. 2009;4(3):263-274.

46. Itkin T, Gur-Cohen S, Spencer JA, et al. Distinct bone marrow blood vessels differentially regulate haematopoiesis. Nature. 2016;532(7599):323-328.

47. Passaro D, Di Tullio A, Abarrategi A, et al. Increased vascular permeability in the bone marrow microenvironment contributes to disease progression and drug response in acute myeloid leukemia. Cancer Cell. 2017;32(3):324-341.

48. Morita Y, Iseki A, Okamura S, Suzuki S, Nakauchi H, Ema H. Functional characterization of hematopoietic stem cells in the spleen. Exp Hematol. 2011;39(3):351-359.

49. De Angulo G, Yuen C, Palla SL, Anderson PM, Zweidler-McKay PA. Absolute lymphocyte count is a novel prognostic indicator in ALL and AML: implications for risk stratification and future studies. Cancer. 2008;112(2):407-415.

Figure legends

Figure 1: Leukemia results in migration of phenotypic stem cells to the spleen. (A) Schematic overview of the leukemia model. In vivo-expanded primary leukemia cells from *Pax5*$^{+/-}$*Ebf1*$^{+/-}$ mice (150,000-200,000) were transplanted into non-conditioned animals. Spleen or BM cells were collected 18-21 days after injection with PBS (PBS) or leukemia cells (TM). (B) Spleen cellularity and tumor burden (CD19^{+} CD45.2^{+} cells) in the spleen 21 days after PBS injection (PBS) (n=8) or transplantation of leukemia cells (TM) (n=9). (C) Frequency and absolute numbers of recipient (CD45.1^{+}) progenitor cell populations in the spleen 21 days after leukemia cell transplantation, determined by FACS analysis. (for specific markers used, see supplementary M&M section and Figure S1C and Table S1) (PBS injected n=8, tumor injected n=9). (D) Representative plots to show the gating used for high-resolution FACS analysis and (E) quantification of the composition of the LSK compartment in BM and spleen from mice injected with PBS (PBS) or B-ALL cells (TM). Long term (LT)-HSCs are defined as LSK CD150^{+} CD48^{-} EPCR(CD201)$^{+}$, Short term (ST) HSCs are defined as LSK CD150^{-} CD48^{-}, MPP2 cells (CD150^{+} CD48^{+}) and a lower frequency of LMPP3/4 cells (CD150^{-} CD48^{+}) (n=8 controls and 7 leukemic mice).

Figure 2: The phenotypic stem cells in leukemic spleen represents multipotent cells with long term reconstitution capacity. (A) Schematic drawing presenting the experimental design to investigate cloning frequency of single phenotypic progenitors in controls and mice transplanted with primary tumor cells *Pax5*$^{+/-}$*Ebf1*$^{+/-}$ mice. LT-HSC (LSK CD150^{+} CD48^{-} CD201^{+}), ST-HSCs (LSK CD150^{-} CD48^{-}) and MPPs (LSK CD48^{+}) from BM and spleen in control (PBS) and leukemic mice (TM). (B) Diagrams displaying the cloning frequency after

seeding of 30 BM or spleen progenitor cells each from 3 controls and 4 leukemic mice as in (A). For control spleen LT-HSCs only 12 cells/sample were seeded. Each dot represents one mouse, and the statistical analysis is performed using two-way Anova. *p<0.05, **p<0.01. (C) Diagrams showing the generation of total CD45.1$^+$ cells, CD19$^+$ B cells, CD3$^+$ T cells, and Gr1$^+$/Mac1$^+$ myeloid cells over 24 weeks after transplantation of 50 LSK CD150$^+$ CD48$^-$ EPCR$^+$ cells from spleen or BM of control mice and mice transplanted with leukemia cells (n = 7-10) to lethally irradiated (9 Gy) CD45.2 mice. (D) Frequency and absolute numbers of hematopoietic progenitors in BM originating from the transplanted HSCs (Panel E) from normal and leukemic donor mice (n=7-10). Statistical analysis was performed using Student's t-test: * $p < 0.05$, ** $p < 0.01$.

Figure 3: Spleen cells maintain their molecular phenotype in leukemia. (A) UMAP generated from scRNA-seq data obtained from Lin$^-$ (CD45, B220, Ter119, CD11b, CD11c, NK1.1, CD3) CD45.1$^-$ CD45.2$^-$ CD19$^-$ CD71$^-$ spleen cells, highlighting the distribution of cells from 1502 control (blue) and 2309 leukemic (*Pax5*$^{+/-}$*Ebf1*$^{+/-}$) (orange) spleen. The defined Leiden clusters are indicated. (B) Heatmap indicating RNA expression levels of markers of non-hematopoietic populations in the spleen. Expression values represent the average of ten centrally ranked cells within each cluster.

Figure 4: HSCs occupies an endothelial niche in normal and leukemic spleen. (A) Representative fluorescence images of spleens from control and leukemic (TM) mice 21 days after leukemia transplantation (*Pax5*$^{+/-}$*Ebf1*$^{+/-}$) or PBS injection, stained with anti-EPCR (CD201) (cyan), anti-CD48 (magenta), and anti-CD31 (green). Arrowheads indicate HSCs (EPCR$^+$ CD48$^-$); arrows indicate EPCR$^+$ CD48$^+$ progenitor cells. (B) Quantification of EPCR$^+$ CD48$^-$ progenitor cells in spleens from control and leukemic (TM) mice. (n=15-20 fields) (C)

Quantification of the distance between EPCR/CD201^{+} hematopoietic progenitors and endothelial (CD31^{+}) cells. Distances from endothelial cells were categorized as 0 µm (direct contact), 1-14 µm (very close), 14-70 µm (close), and >70 µm (far). Statistical analysis was performed using Student's t-test: * $p < 0.05$, ** $p < 0.01$.

Figure 5: Leukemia impact gene expression patterns in bone marrow niche cells. (A) UMAP generated from scRNA-seq data of cells positive (M+) for any of the following markers: CD31, CD34, CD44, CD51, CD106, CD114, CD140a, Sca1, or LEPR, and negative for CD71, CD19, CD11b, B220, Ter119, and CD45. The plot highlights the distribution of cells from control (blue) and leukemic (TM) (*Pax5*$^{+/-}$*Ebf1*$^{+/-}$) (orange) BM. The numbers in the UMAP indicate the defined Leiden clusters. (B) Heatmap showing RNA expression levels of markers of non-hematopoietic BM populations. Expression values represent the average of ten cells centered within the distribution of values for each cluster.

Figure 6: Leukemia progression induces a shift in Cxcl12 gradients. (A) Heatmaps indicating RNA expression levels of cytokine-encoding genes in the BM and spleen of normal and leukemic mice. Expression values represent the average of ten centrally ranked cells within each cluster. (B) Leukemia cells as a percentage of total cells in BM, spleen, and peripheral blood (PB) at days 6, 10, and 14 after transplantation of 150,000 leukemia cells (*Pax5*$^{+/-}$*Ebf1*$^{+/-}$) (n = 5). Leukemia cell frequencies were compared with tissue-specific healthy controls (n = 9) using FACS analysis to identify CD45.2^{+} cells. Statistical analysis: one-way ANOVA; *** $p < 0.001$, **** $p < 0.0001$. (C) Normalized CXCL12 concentrations in BM and spleen at days 6, 10, and 14 after leukemia cell transplantation (n = 5), measured by ELISA. Values were normalized to the CXCL12 levels detected in BM or spleen in PBS injected healthy controls (n = 9). Statistical significance in relative reduction between leukemic tissues was assessed

using Student's t-test; * $p < 0.05$, ** $p < 0.01$. (D) Frequency of LSK cells in the spleen or BM (frequency and absolute number) of healthy control mice (n = 9) compared with leukemic mice at days 6, 10, and 14 after leukemia cell transplantation (n = 5 at each time point), as determined by FACS analysis. Statistical analysis: one-way ANOVA; *** $p < 0.001$, **** $p < 0.0001$.

Figure 7: BM resilience upon removal of leukemic cells. (A) Schematic overview of the leukemia model developed to enable doxycycline (Dox)-induced deletion of leukemic cells. Trans-heterozygous *Pax5*/*Ebf1* mice were crossed with a Cas9-inducible mouse line (*Pax5*$^{+/-}$ *Ebf1*$^{+/-}$*iCAS9*$^{+}$) to generate iCas9-inducible B-ALL cells. These B-ALL cells were transduced with either a control gRNA (R26) or gRNAs designed to introduce multiple genomic cuts and induce cell death ("Killswitch"; KS). Transduced B-ALL cells were transplanted into recipient mice, and once the mice became leukemic, Dox was administered to eliminate the leukemia, allowing analysis of hematopoietic recovery without chemotherapy. (B) Frequency of leukemia cells in BM and spleen at Day 14 after transplantation (Day 0) and at 4, 8, and 14 days after induction of iCas9 expression by intraperitoneal Dox injection (n = 4–6). (C) Progenitor cell numbers in the BM of Dox-treated mice at the indicated time points after initiation of Dox administration (n = 4-6). Statistical analysis: Student's t-test; * $p < 0.05$, ** $p < 0.01$, *** $p < 0.001$, **** $p < 0.0001$. (D) Relative abundance of LT-HSCs in the spleen of control and leukemic Dox-treated mice at Day 14 after transplantation (Day 0) and at 4, 8, and 14 days after induction of iCas9 expression by intraperitoneal Dox injection (n = 4-5).

Figure 8: Depletion of leukemic cells in B-ALL patients results in restoration of hematopoiesis in the BM. (A) Representative UMAP showing recovery of human BM cell populations from treatment initiation (NOPHO2008 protocol, Day 0) to the first evaluation time point (Day 15) in patients with CD19^{+} B-ALL. Cells were clustered based on surface

antigen expression. (B) Frequency of $CD19^+$ B-ALL cells, defined as cells populating $CD19^+$ clusters present in leukemia samples but absent in controls, throughout the treatment period (Days 0, 15, 29, 78-79), as determined by FACS analysis. Statistical analysis: one-way ANOVA; * $p < 0.05$, ** $p < 0.01$, *** $p < 0.001$, **** $p < 0.0001$. (C) BM cell populations in B-ALL patients throughout treatment (Days 0, 15, 29, 78-79) (n = 15), compared to controls (31) (n = 9). Lineage-negative (Lin^-) progenitor cells were defined as $CD45^+$ $CD34^+$ $CD38^+$ $CD19^-$ $CD20^-$ $CD22^-$ $CD66c^-$. Myeloid lineage cells were defined as $CD45^+$ $CD19^-$ $CD20^-$ $CD22^-$ with expression of CD38 and/or CD66c. The erythroid lineage was defined as $CD10^-$ $CD19^-$ $CD20^-$ $CD22^-$ $CD45^-$ $CD66c^-$ and the Lymphoid lineages as $CD45^+$ $CD66c^-$ with expression of CD10, CD19, CD20, or CD22. Statistical analysis: one-way ANOVA; * $p < 0.05$, ** $p < 0.01$.

Figure 1

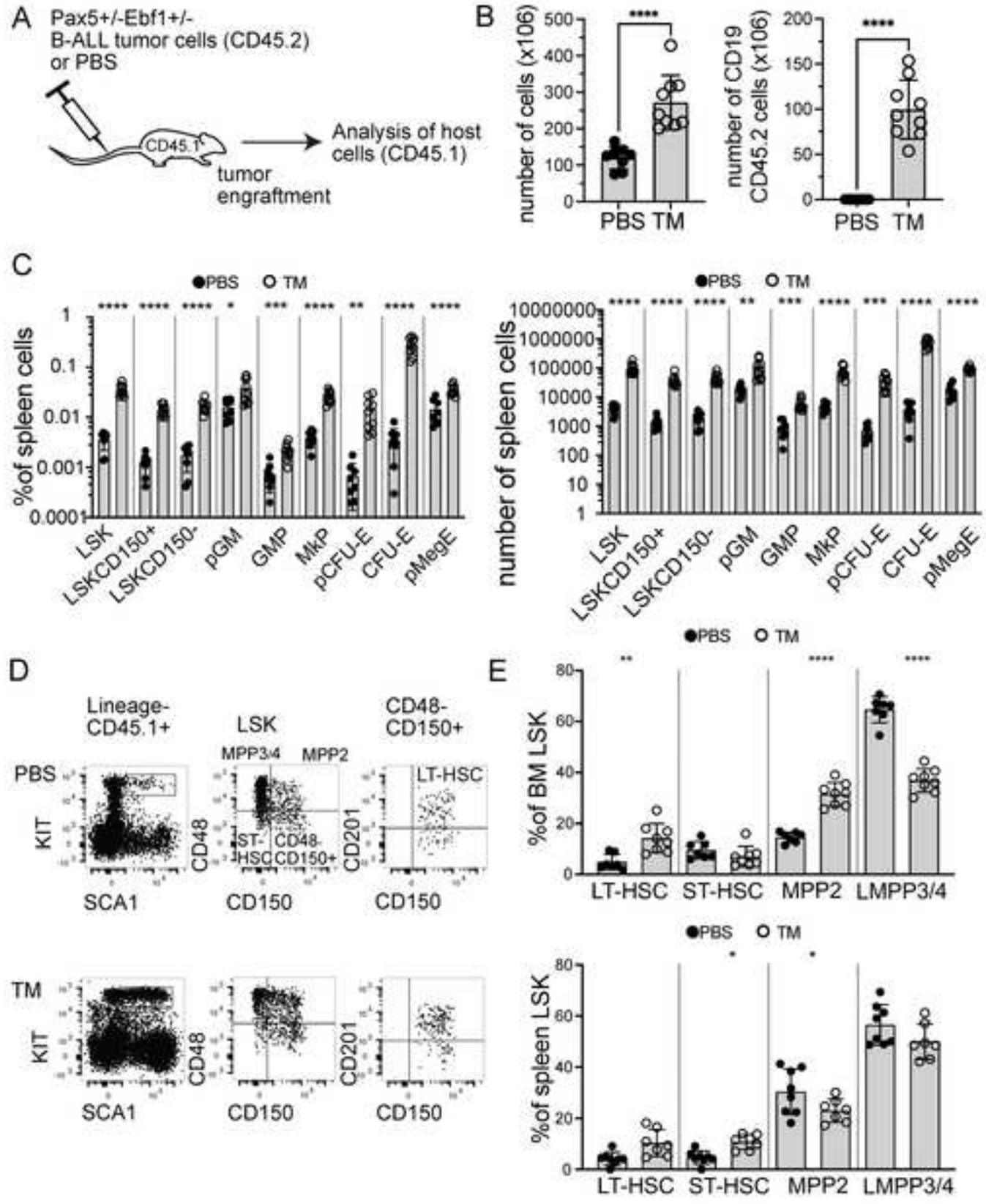
A
Pax5+/-Ebf1+/-
B-ALL tumor cells (CD45.2)
or PBS
CD45.1
tumor
engraftment
Analysis of host
cells (CD45.1)
B
number of cells (x106)
PBS TM
number of CD19
CD45.2 cells (x106)
PBS TM
C
PBS TM
%of spleen cells
number of spleen cells
LSK
LSKCD150+
LSKCD150-
pGM
GMP
MkP
pCFU-E
CFU-E
pMegE
D
Lineage-
CD45.1+
LSK
CD48-
CD150+
MPP3/4
MPP2
LT-HSC
ST-HSC
CD48-
CD150+
PBS
TM
KIT
SCA1
CD48
CD150
CD201
E
PBS TM
%of BM LSK
%of spleen LSK
LT-HSC
ST-HSC
MPP2
LMPP3/4

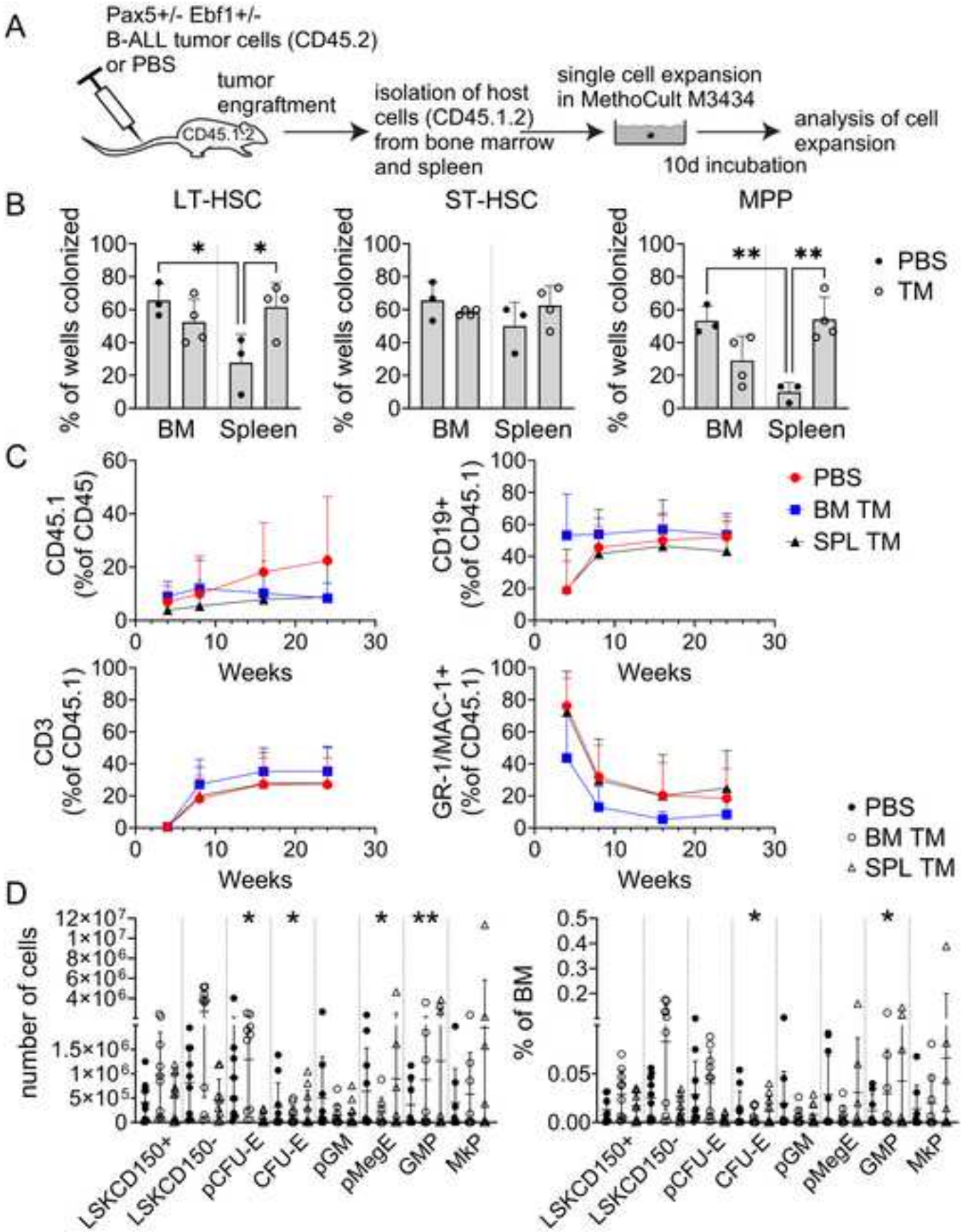
A
Pax5+/- Ebf1+/-
B-ALL tumor cells (CD45.2)
or PBS
tumor
engraftment
CD45.1.2
isolation of host
cells (CD45.1.2)
from bone marrow
and spleen
single cell expansion
in MethoCult M3434
10d incubation
analysis of cell
expansion
B
LT-HSC
ST-HSC
MPP
% of wells colonized
BM
Spleen
PBS
TM
C
CD45.1
(%of CD45)
CD19+
(%of CD45.1)
CD3
(%of CD45.1)
GR-1/MAC-1+
(%of CD45.1)
Weeks
PBS
BM TM
SPL TM
D
number of cells
% of BM
LSKCD150+
LSKCD150-
pCFU-E
CFU-E
pGM
pMegE
GMP
MkP

Figure 3

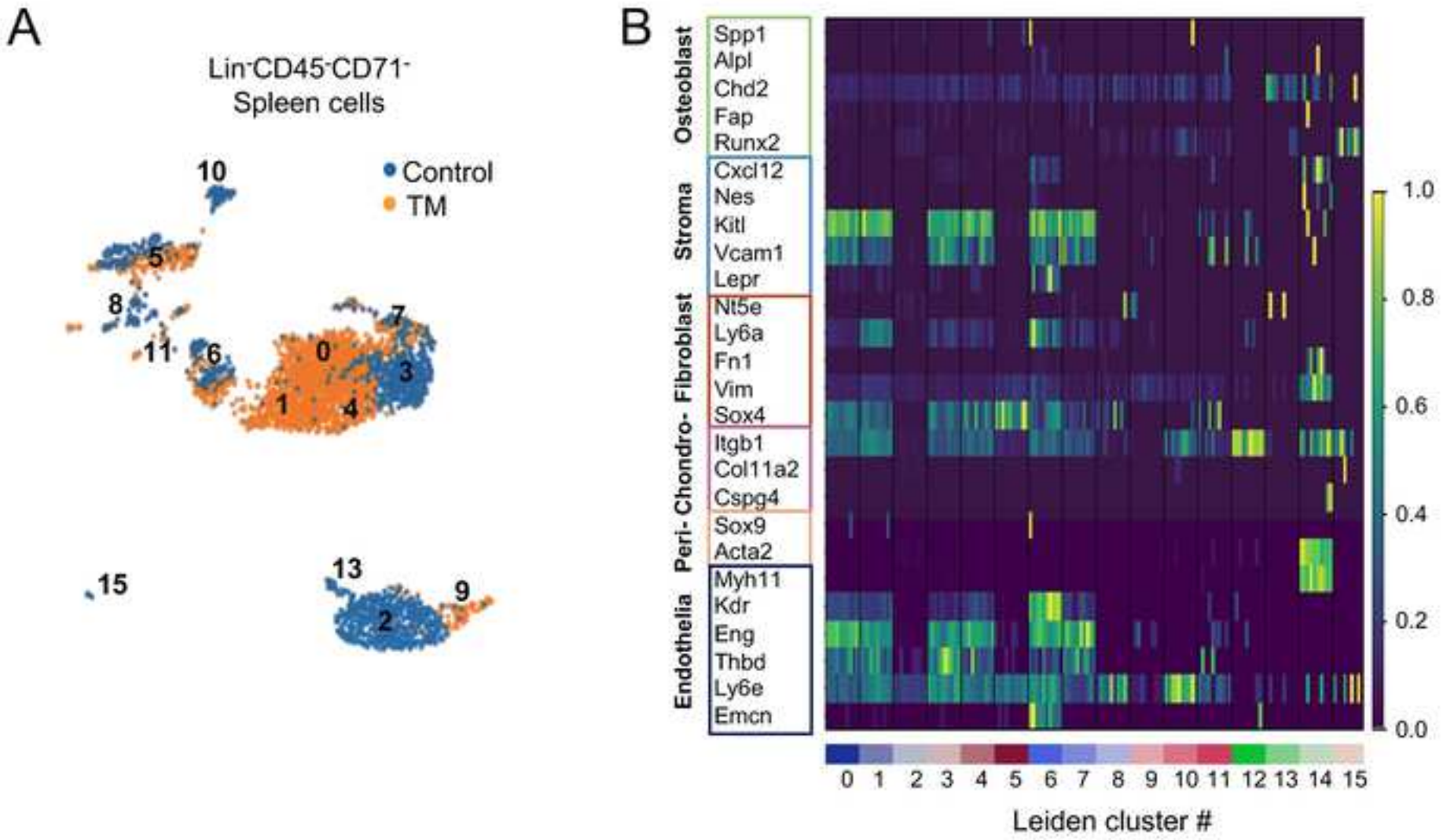
A
Lin-CD45-CD71-
Spleen cells
Control
TM
10
5
8
11
6
7
0
3
1
4
15
13
9
2
B
Osteoblast
Spp1
Alpl
Chd2
Fap
Runx2
Stroma
Cxcl12
Nes
Kitl
Vcam1
Lepr
Fibroblast
Nt5e
Ly6a
Fn1
Vim
Sox4
Chondro-
Itgb1
Col11a2
Cspg4
Peri-
Sox9
Acta2
Endothelia
Myh11
Kdr
Eng
Thbd
Ly6e
Emcn
1.0
0.8
0.6
0.4
0.2
0.0
0 1 2 3 4 5 6 7 8 9 10 11 12 13 14 15
Leiden cluster #

Figure 4

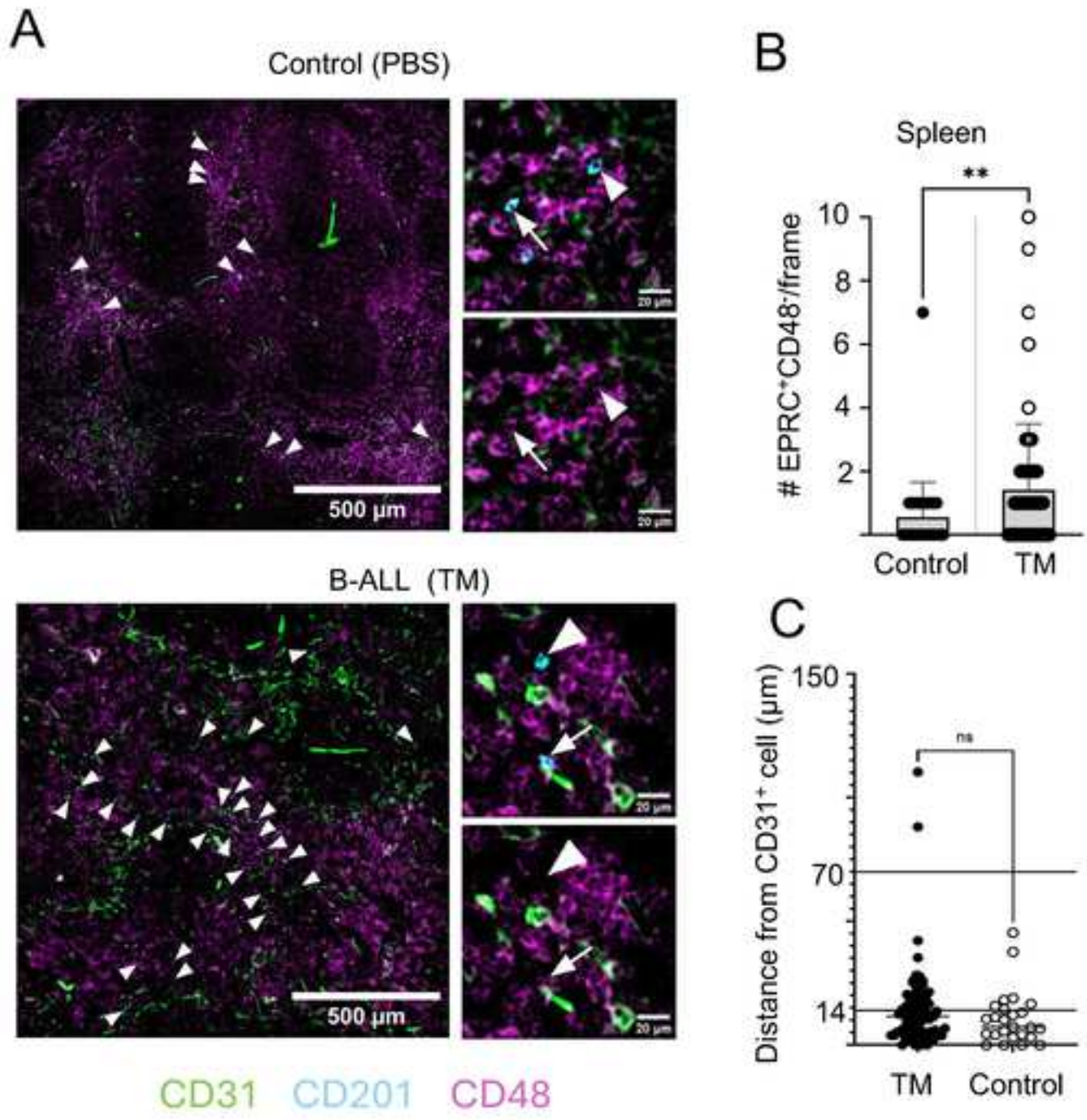
A
Control (PBS)
500 µm
B-ALL (TM)
500 µm
CD31 CD201 CD48
B
Spleen
**
EPRC+CD48-/frame
10
8
6
4
2
Control
TM
C
Distance from CD31+ cell (µm)
150
70
14
ns
TM
Control

Figure 5

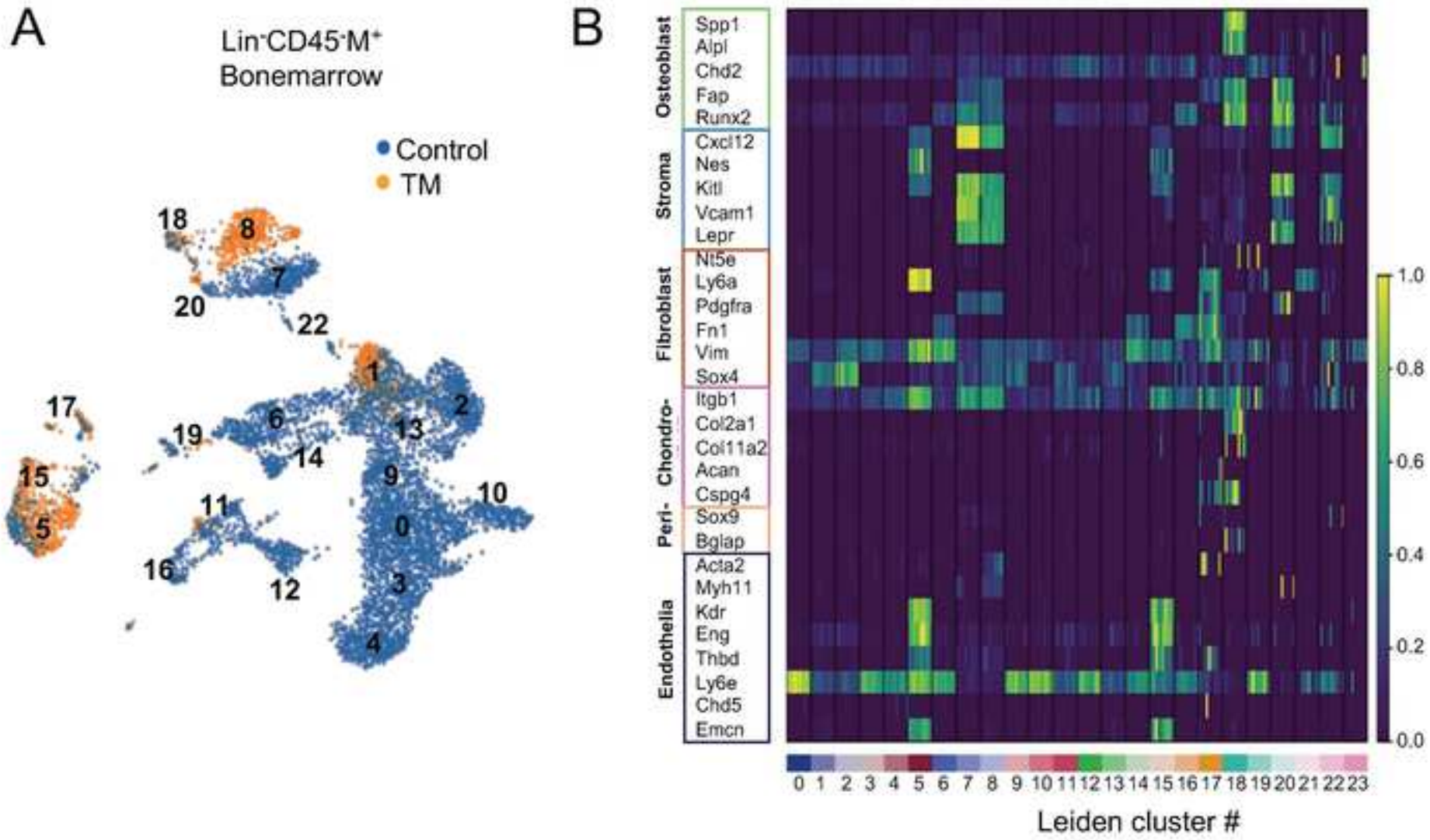
A
Lin-CD45-M+
Bonemarrow
Control
TM
18
8
7
20
22
1
2
17
19
6
13
14
15
9
10
11
0
5
16
12
3
4
B
Osteoblast
Spp1
Alpl
Chd2
Fap
Runx2
Stroma
Cxcl12
Nes
Kitl
Vcam1
Lepr
Fibroblast
Nt5e
Ly6a
Pdgfra
Fn1
Vim
Sox4
Chondro-
Itgb1
Col2a1
Col11a2
Acan
Cspg4
Peri-
Sox9
Bglap
Endothelia
Acta2
Myh11
Kdr
Eng
Thbd
Ly6e
Chd5
Emcn
1.0
0.8
0.6
0.4
0.2
0.0
0 1 2 3 4 5 6 7 8 9 10 11 12 13 14 15 16 17 18 19 20 21 22 23
Leiden cluster #

Figure 6

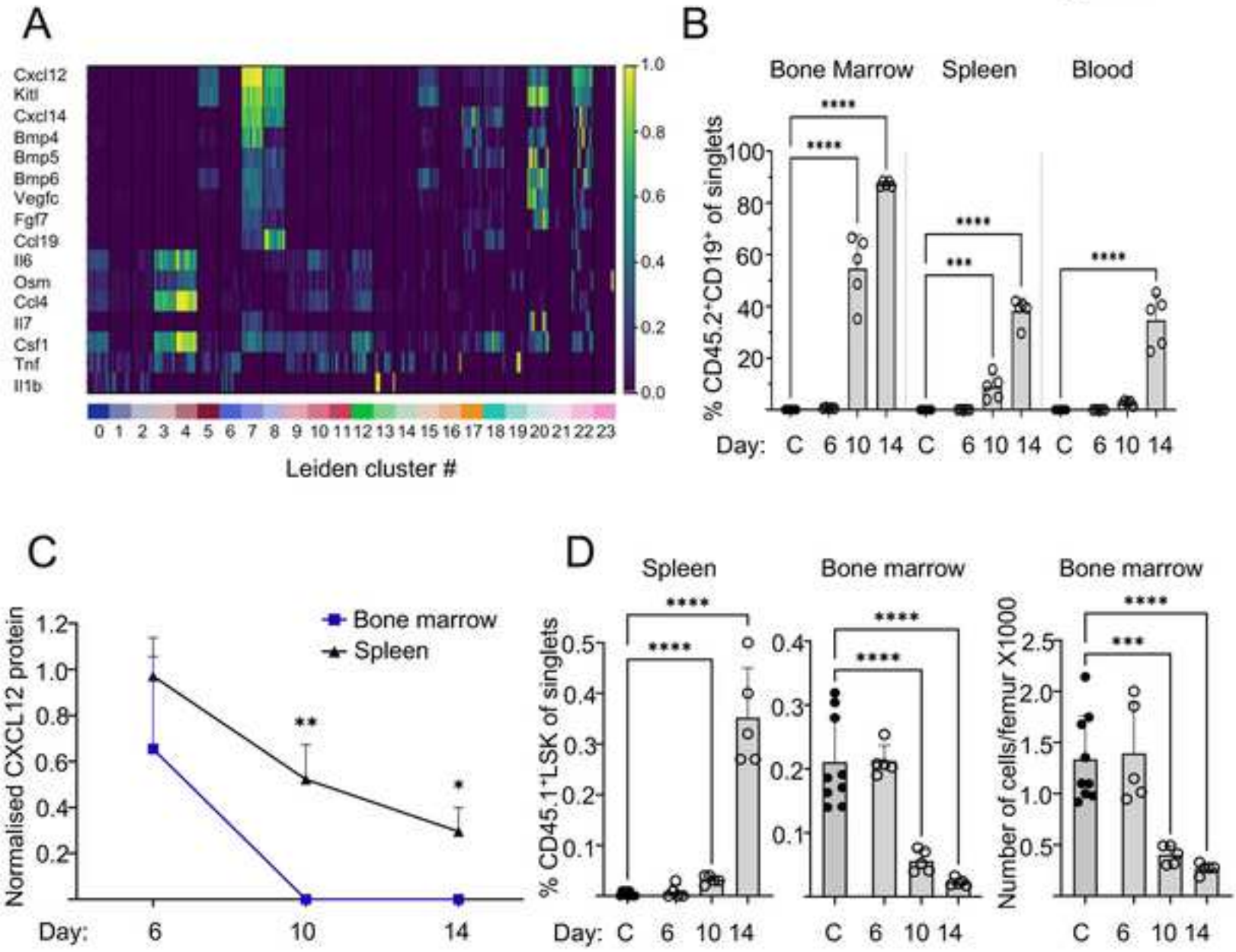
A
Cxcl12
Kitl
Cxcl14
Bmp4
Bmp5
Bmp6
Vegfc
Fgf7
Ccl19
Il6
Osm
Ccl4
Il7
Csf1
Tnf
Il1b
1.0
0.8
0.6
0.4
0.2
0.0
0 1 2 3 4 5 6 7 8 9 10 11 12 13 14 15 16 17 18 19 20 21 22 23
Leiden cluster #
B
Bone Marrow
Spleen
Blood
% CD45.2+CD19+ of singlets
Day: C 6 10 14 C 6 10 14 C 6 10 14
C
Normalised CXCL12 protein
Bone marrow
Spleen
Day: 6 10 14
D
Spleen
Bone marrow
Bone marrow
% CD45.1+LSK of singlets
Number of cells/femur X1000
Day: C 6 10 14

Figure 7

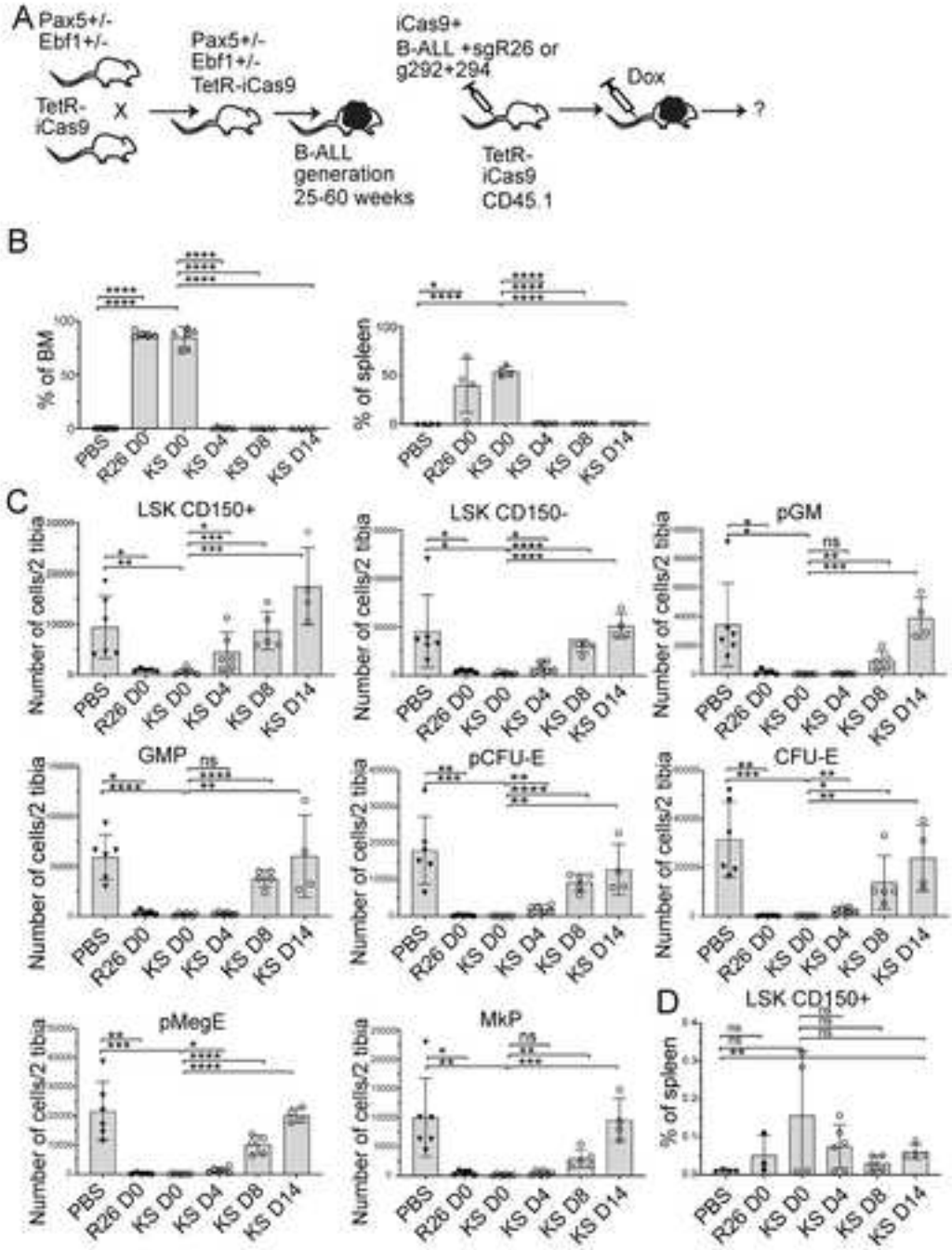
A
Pax5+/-
Ebf1+/-
TetR-
iCas9
X
Pax5+/-
Ebf1+/-
TetR-iCas9
B-ALL
generation
25-60 weeks
iCas9+
B-ALL +sgR26 or
g292+294
TetR-
iCas9
CD45.1
Dox
?
B
% of BM
% of spleen
PBS
R26 D0
KS D0
KS D4
KS D8
KS D14
C
LSK CD150+
LSK CD150-
pGM
GMP
pCFU-E
CFU-E
pMegE
MkP
Number of cells/2 tibia
ns
D
LSK CD150+
% of spleen

Figure 8

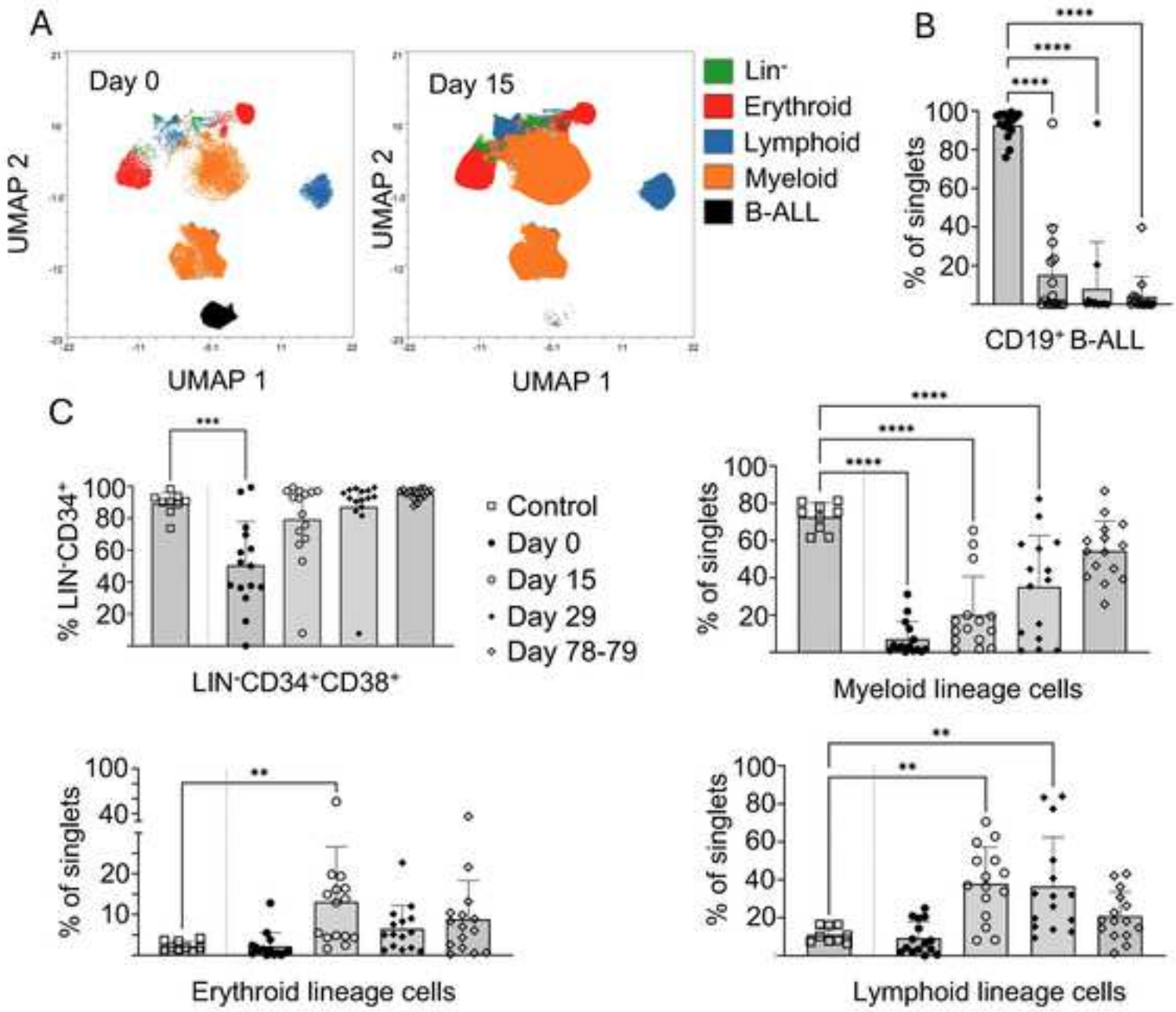
A
Day 0
Day 15
UMAP 2
UMAP 1
Lin-
Erythroid
Lymphoid
Myeloid
B-ALL
B
% of singlets
CD19+ B-ALL
C
% LIN-CD34+
LIN-CD34+CD38+
Control
Day 0
Day 15
Day 29
Day 78-79
Myeloid lineage cells
Erythroid lineage cells
Lymphoid lineage cells

Figure S1

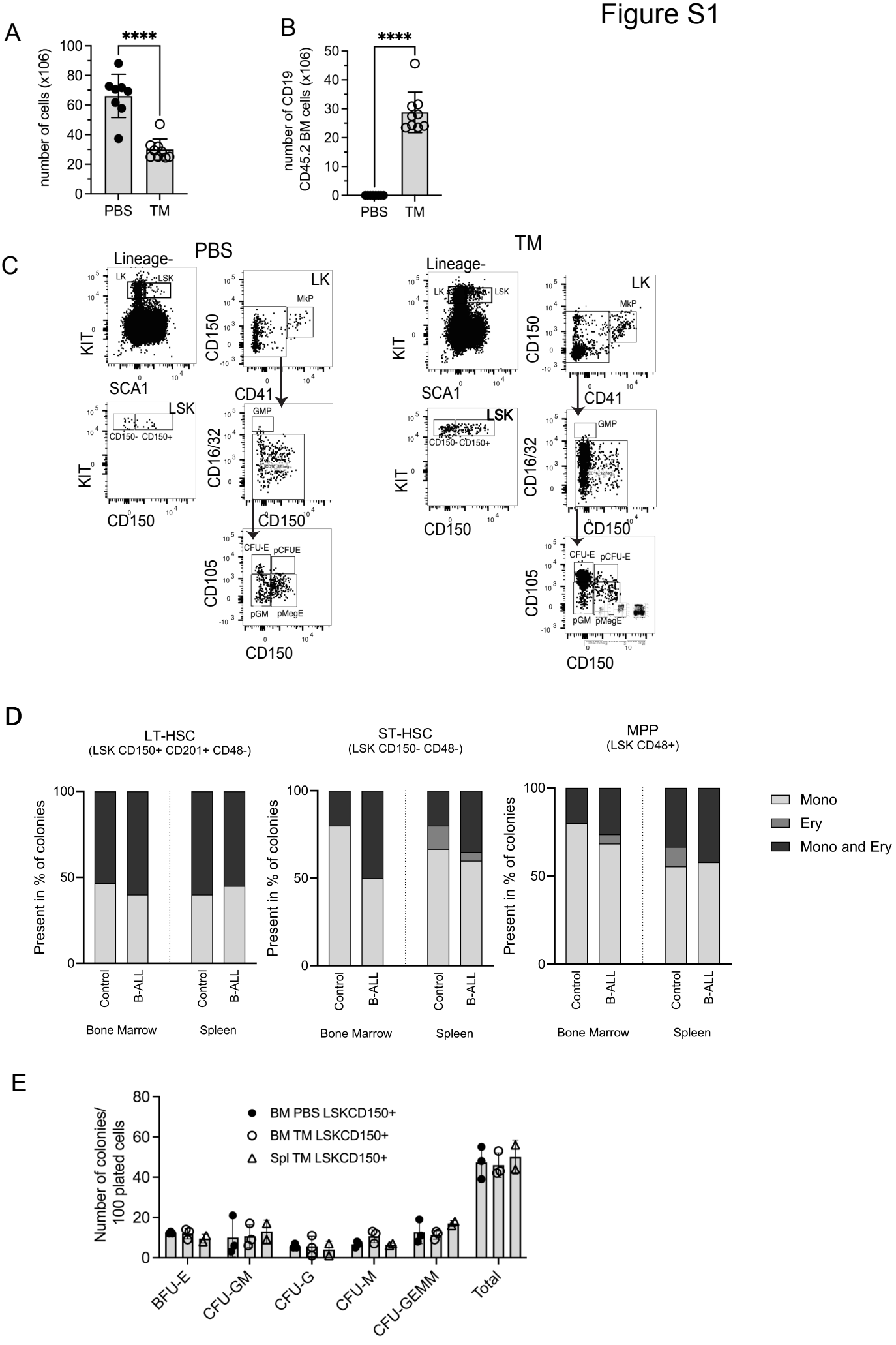
A
number of cells (x106)
****
PBS
TM
B
number of CD19 CD45.2 BM cells (x106)
****
PBS
TM
C
PBS
TM
Lineage-
LK
LSK
KIT
SCA1
MkP
CD150
CD41
GMP
CD16/32
CD105
CFU-E
pCFUE
pCFU-E
pGM
pMegE
D
LT-HSC
(LSK CD150+ CD201+ CD48-)
ST-HSC
(LSK CD150- CD48-)
MPP
(LSK CD48+)
Present in % of colonies
Control
B-ALL
Bone Marrow
Spleen
Mono
Ery
Mono and Ery
E
Number of colonies/ 100 plated cells
BM PBS LSKCD150+
BM TM LSKCD150+
Spl TM LSKCD150+
BFU-E
CFU-GM
CFU-G
CFU-M
CFU-GEMM
Total

Figure S1: Leukemia cause extramedullary hematopoiesis. (A-B) Diagrams showing the absolute number of cells in the BM (A) and the number of leukemia cells (B) 21 days after transplantation of 150,000 *Pax5*$^{+/-}$*Ebf1*$^{+/-}$ leukemia cells (TM) or injection of PBS (PBS). (n=8-9)(C) Representative FACS plots illustrating how progenitor populations were defined in control (PBS) and leukemic (TM) spleen. Lineage negative SCA^{+} KIT^{+} (LSK) cells, CD150^{+} LSK, long term stem cells (LT-HSC), CD150^{-} LSK, short term stem cells, pro-granulocyte/monocyte progenitors (pGM), granulocyte/monocyte progenitors (GMP), pre-megakaryocyte/erythrocyte progenitor (pMegE), megakaryocyte progenitors (MkP), pre-colony forming unit erythroid cells (pCFU-E) and colony forming erythroid (CFU-E). (D) Diagrams displaying the cellular content in wells generated from single cell cloning of long term (LT)-HSCs, short term (ST)-HSCs or Mulitpotent progenitors (MPPs) from control or leukemic mice (B-ALL). Cell identity was determined by FACS analysis defining monocytes CD45^{+} CD11b^{+} CD16/32^{+} Ly6c^{+}) and erythroid cells (CD45$^{low/neg}$ CD71^{+}). The data are based on analysis of 5 single cell clones from each population and mouse (n=3 controls and 4 Leukemic mice) (E) Output of myeloid colonies after in vitro incubation of CD150^{+} HSCs from control BM (PBS) or leukemic BM and spleen (n = 2-3). BFU-E, burst-forming unit-erythroid; CFU-GM, colony-forming unit-granulocyte/monocyte; CFU-G, colony-forming unit-granulocyte; CFU-M, colony-forming unit-monocyte; CFU-GEMM, colony-forming unit-granulocyte/erythrocyte/monocyte/megakaryocyte. Statistical analysis was performed using Student's t-test: **** $p < 0.0001$.

Figure S2

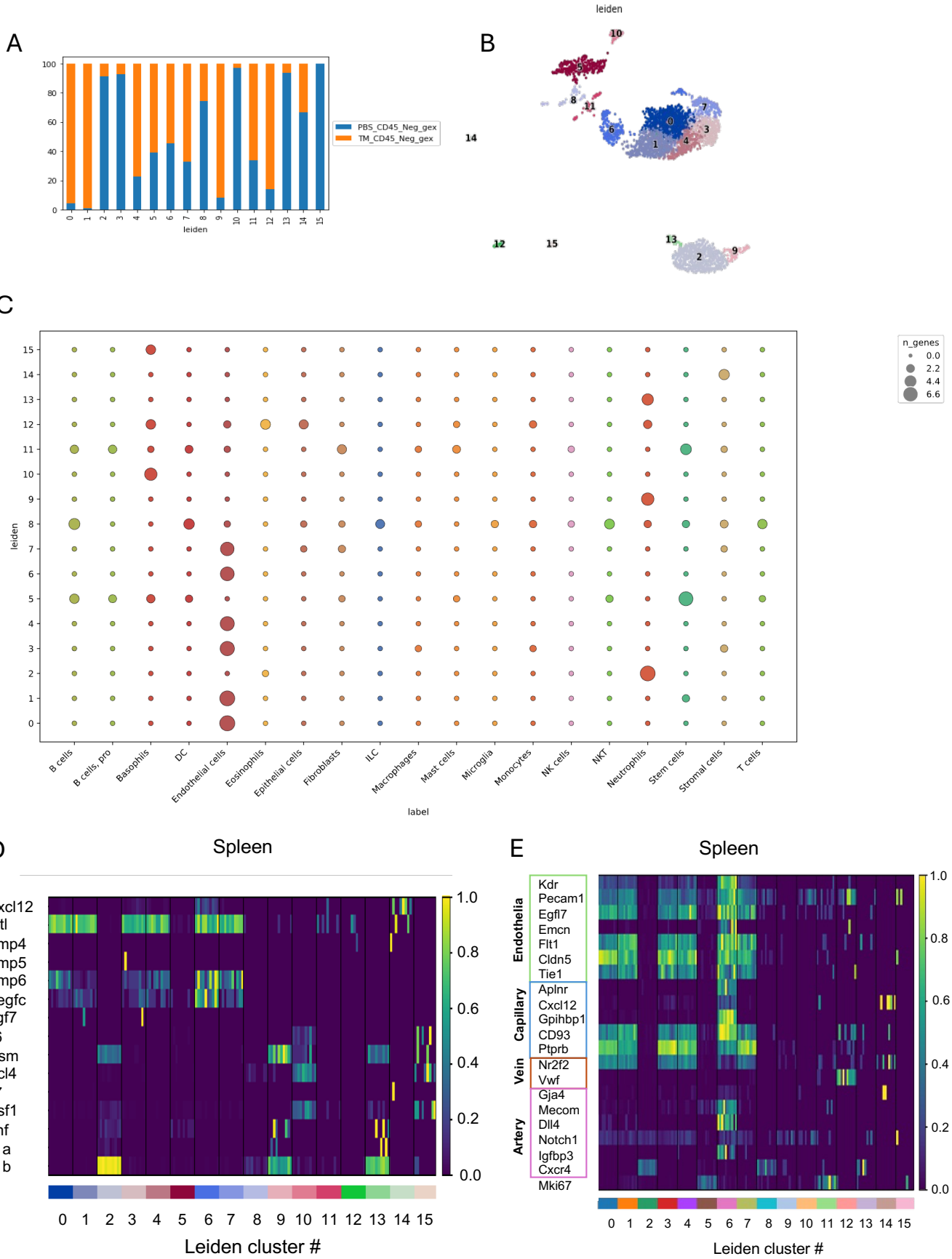
A
PBS_CD45_Neg_gex
TM_CD45_Neg_gex
leiden
B
leiden
C
n_genes
0.0
2.2
4.4
6.6
leiden
label
B cells
B cells, pro
Basophils
DC
Endothelial cells
Eosinophils
Epithelial cells
Fibroblasts
ILC
Macrophages
Mast cells
Microglia
Monocytes
NK cells
NKT
Neutrophils
Stem cells
Stromal cells
T cells
D
Spleen
Cxcl12
Kitl
Bmp4
Bmp5
Bmp6
Vegfc
Fgf7
Il6
Osm
Ccl4
Il7
Csf1
Tnf
Il1a
Il1b
Leiden cluster #
E
Spleen
Endothelia
Capillary
Vein
Artery
Kdr
Pecam1
Egfl7
Emcn
Flt1
Cldn5
Tie1
Aplnr
Cxcl12
Gpihbp1
CD93
Ptprb
Nr2f2
Vwf
Gja4
Mecom
Dll4
Notch1
Igfbp3
Cxcr4
Mki67
Leiden cluster #

Figure S2: Cells in leukemic spleen maintains their molecular identity. (A) Diagram showing the percentage of PBS and TM spleen cells assigned to each defined Leiden cluster. (B) UMAP showing the defined Leiden clusters in splenic populations. (C) Single R based Heatmaps indicating the expression of tissue-restricted genes across the defined clusters. (D) Heatmaps indicating RNA expression levels of cytokine-encoding genes in the spleen of normal and leukemic mice. Expression values represent the average of ten centrally ranked cells within each cluster. (E) Heatmap displaying expression levels of endothelial marker genes, calculated from ten centrally ranked cells within each cluster.

A

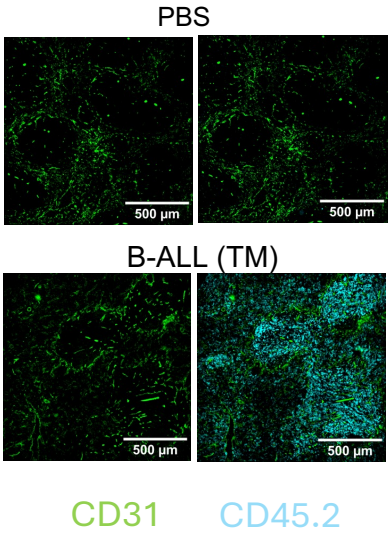
PBS
500 µm
500 µm
B-ALL (TM)
500 µm
500 µm
CD31
CD45.2

B

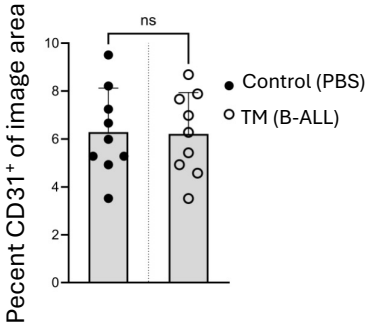
ns
Pecent CD31⁺ of image area
10
8
6
4
2
0
Control (PBS)
TM (B-ALL)

Figure S3: Endothelial cells constitute the HSC niche in leukemic spleen. (A) Representative fluorescence images of spleens from control and leukemia (*Pax5*$^{+/-}$*Ebf1*$^{+/-}$) transplanted mice stained with anti-CD45.2 (cyan) to detect leukemia cells and anti-CD31 (green) to visualize endothelial cells. Magnification 25×. (B) Diagram showing the total number of CD31^{+} cells per section in control (PBS) and leukemia- (TM) transplanted mice 21 days after transplantation (n = 10 images). Statistical analysis was performed using Student's t-test: * $p < 0.05$, ** $p < 0.01$.

Figure S4

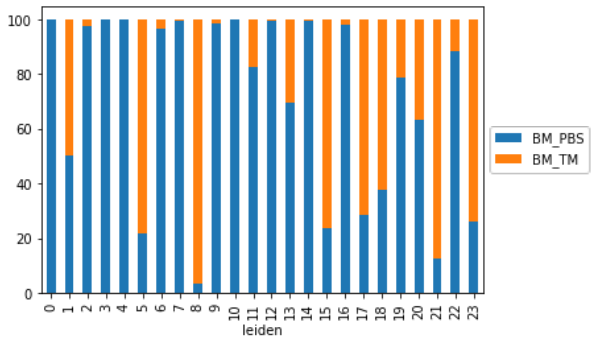
A
BM_PBS
BM_TM
leiden

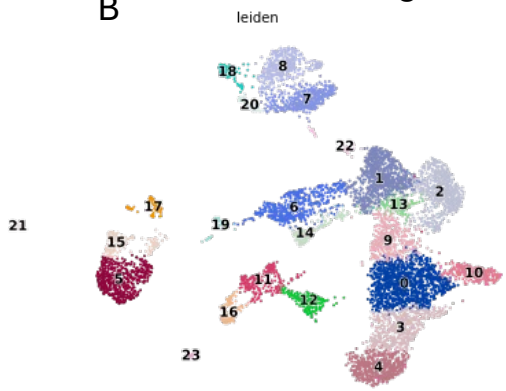
B
leiden

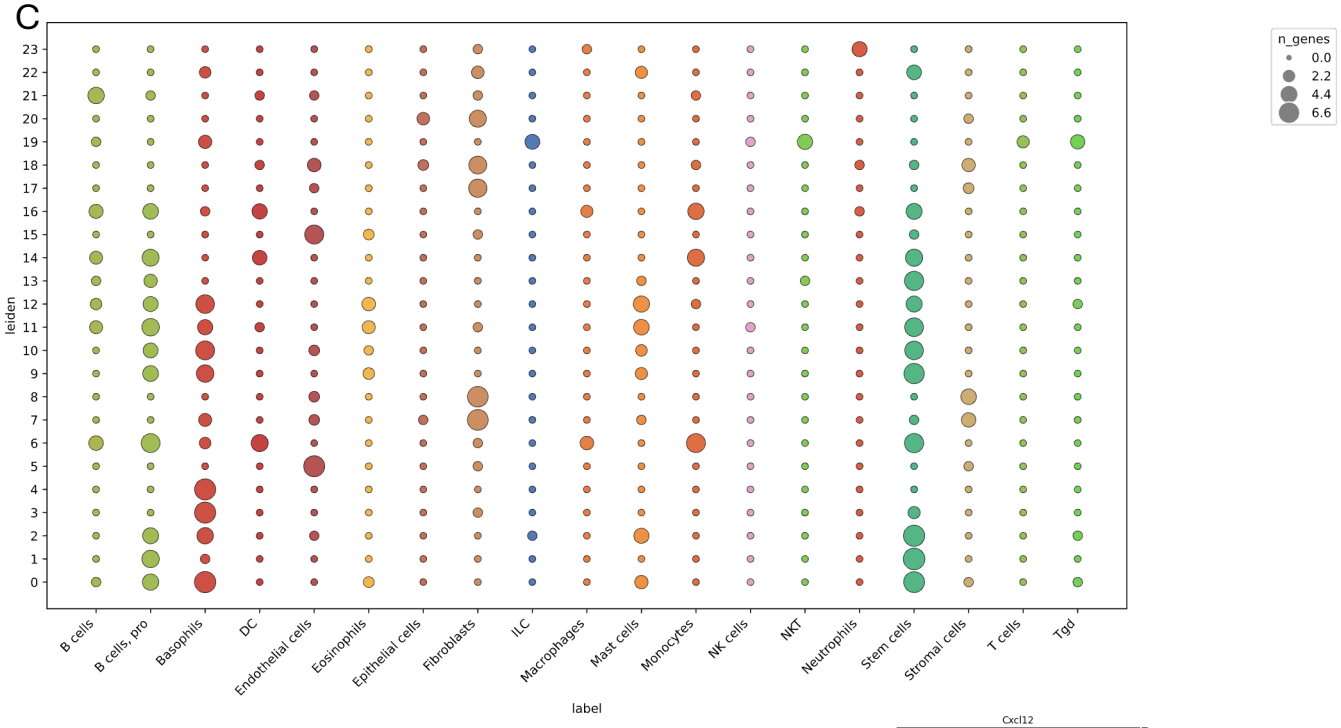
C
n_genes
leiden
label
B cells
B cells, pro
Basophils
DC
Endothelial cells
Eosinophils
Epithelial cells
Fibroblasts
ILC
Macrophages
Mast cells
Monocytes
NK cells
NKT
Neutrophils
Stem cells
Stromal cells
T cells
Tgd

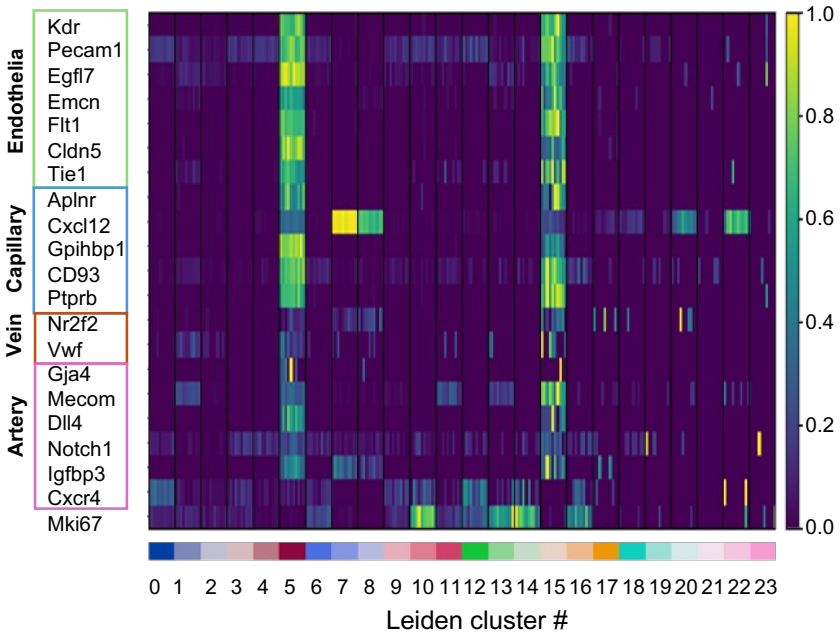
D
Bone marrow
Endothelia
Kdr
Pecam1
Egfl7
Emcn
Flt1
Cldn5
Tie1
Capillary
Aplnr
Cxcl12
Gpihbp1
CD93
Ptprb
Vein
Nr2f2
Vwf
Artery
Gja4
Mecom
Dll4
Notch1
Igfbp3
Cxcr4
Mki67
Leiden cluster #

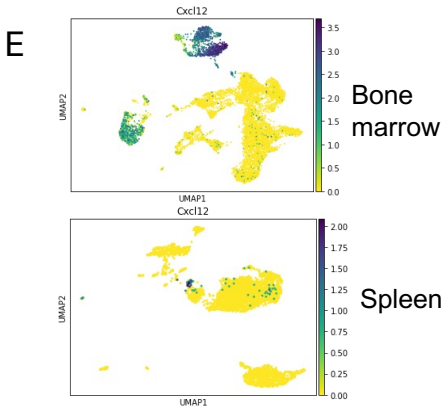
E
Cxcl12
UMAP1
UMAP2
Bone marrow
Spleen

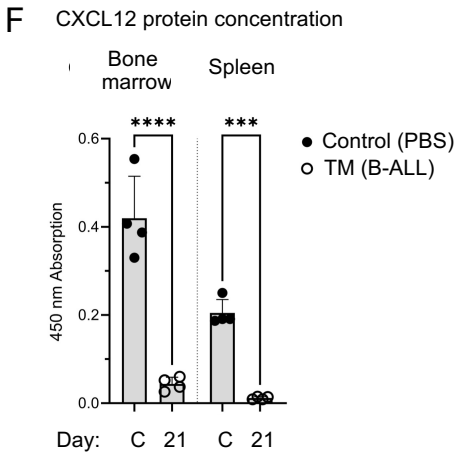
F
CXCL12 protein concentration
Bone marrow
Spleen
****
***
Control (PBS)
TM (B-ALL)
450 nm Absorption
Day: C 21 C 21

Figure S4: Leukemia induce changes to the composition of the BM microenvironment. (A) Diagram showing the percentage of PBS and TM BM cells assigned to each defined Leiden cluster. (B) UMAP showing the defined Leiden clusters in BM populations. (C) Single R based heatmaps indicating the expression of tissue-restricted genes across the defined clusters. (D) Heatmap displaying expression levels of endothelial marker genes, calculated from ten centrally ranked cells within each cluster. (E) UMAP-based heatmaps displaying *Cxcl12* expression in cells collected from BM and spleen of normal and leukemic mice. (F) Diagrams displaying the free protein levels of CXCL12 in BM and spleen in terminally sick animals (Day 21, n=4 animals in each group). Statistical analysis has been made based on Student's t-test. *** $p < 0.001$, **** $p < 0.0001$.

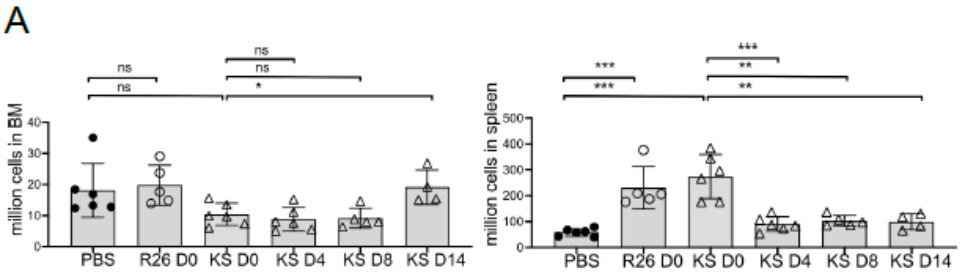
A
million cells in BM
ns
ns
ns
*
PBS
R26 D0
KS D0
KS D4
KS D8
KS D14
million cells in spleen
***
***
***
**
**
PBS
R26 D0
KS D0
KS D4
KS D8
KS D14

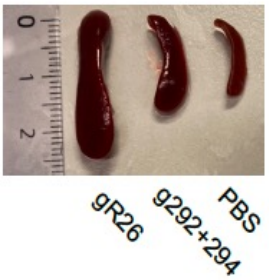
B
gR26
g292+294
PBS

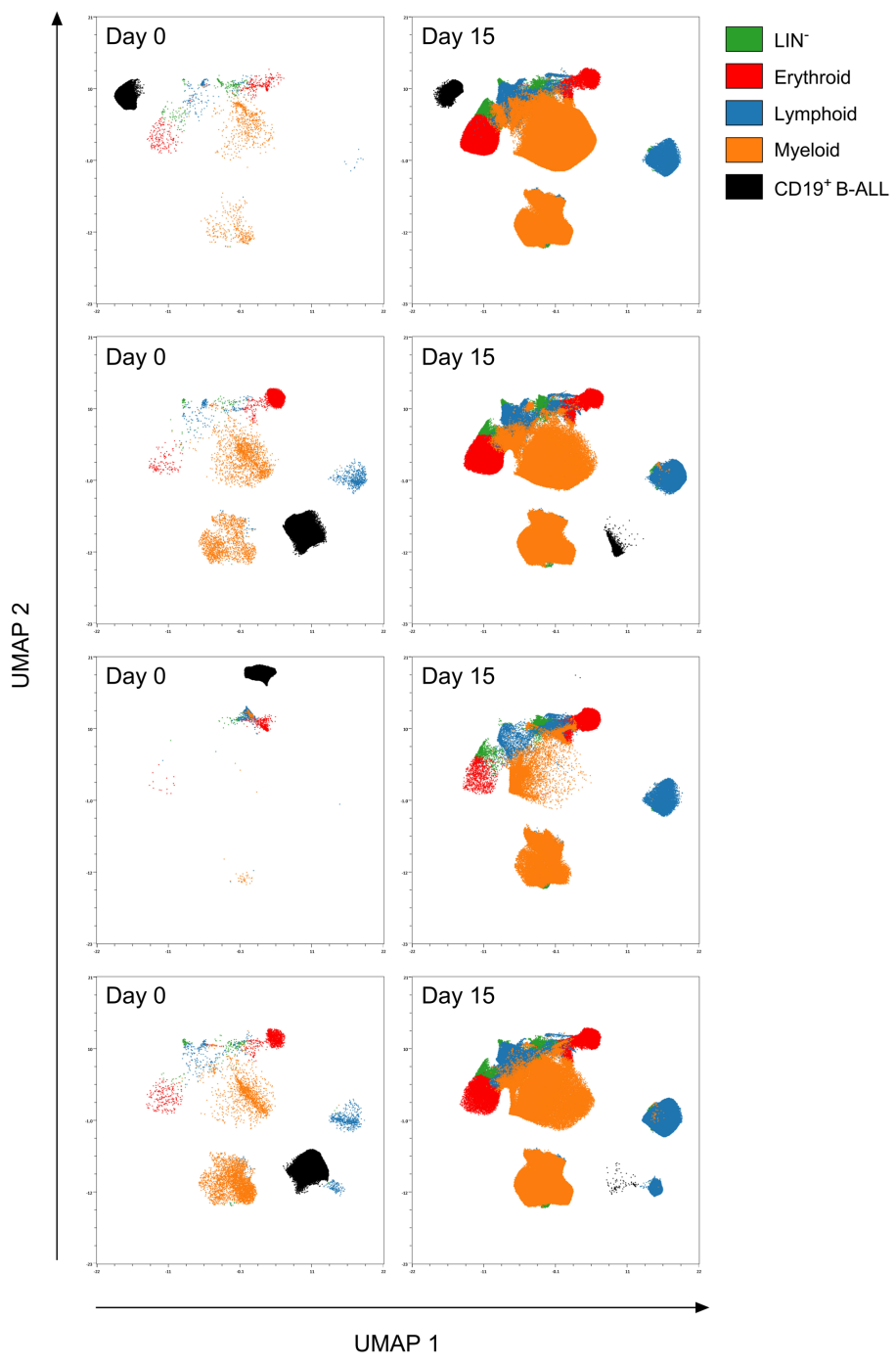
C
Day 0
Day 15
LIN-
Erythroid
Lymphoid
Myeloid
CD19+ B-ALL
UMAP 2
UMAP 1

Figure S5: Recovery after leukemia depletion. (A) Cell counts in BM and spleen following leukemia (*Pax5*$^{+/-}$*Ebf1*$^{+/-}$*iCAS9*$^{+}$) cell depletion. (B) Spleen size in leukemic (gR26), recovered (g292+294), and control (PBS) mice (n = 4-6). Statistical analysis: Student's t-test; * $p < 0.05$, ** $p < 0.01$, *** $p < 0.001$, **** $p < 0.0001$. (C) UMAP projections of BM samples from four CD19^{+} B-ALL patients from treatment initiation (Day 0) to the first evaluation time point (Day 15). Cells are clustered based on surface antigen expression.

Extended Experimental procedures Jensen et al.

Animal models.

Leukemia cells were obtained from *Pax5*$^{+/-}$ *Ebf1*$^{+/-}$ mice (1) on a C57BL/6 (CD45.2) background. Adoptive transfers were performed by tail vein injection of 150,000-200,000 tumor cells in PBS/1%FCS to CD45.1^{+} to C57BL/6 non-conditioned animals. Disease was manifested by palpable accessory axillary- or subiliac- lymph nodes (LN) (2) and splenomegaly within 3-4 weeks after transplantation (1). TetO-Cas9 mice were bought from JAX mice (Stock no: 029476 - B6.Cg-Col1a1<tm1(tetO-cas9)Sho>/J) and crossed with R26m2rtTA mice to obtain a Cas9 inducible (iCas9) mouse line. Cas9 inducible tumor cells were then obtained by crossing the *Pax5*$^{+/-}$ *Ebf1*$^{+/-}$ mice with iCas9 mice. Recipient animals for iCas9 *Pax5*$^{+/-}$ *Ebf1*$^{+/-}$ tumor propagation was generated by crossing iCas9 mice with CD45.1^{+} B6.SJL mice to obtain CD45.1^{+} C57BL/6 recipient mice. Animal procedures were performed with consent from the ethics committees at Lund University (Lund, Sweden) and Linköping University (Linköping, Sweden).

Fluorescence Activated Cell Sorting (FACS).

Bone marrow cells were isolated from the femur of sacrificed mice by crushing the bones in PBS containing 2 % FCS and 0,5 % BSA using a pestle and mortar. Bone fragments were separated from the cell suspension by filtering the solution through a 70 µm nylon mesh, followed by a red blood cell lysis. Spleen cells were isolated by forcing the spleen tissue through a 70 µm nylon mesh and washing cells using PBS containing 2 % FCS and 0,5 % BSA, followed by a red blood cell lysis. Samples were subjected to red blood cell lysis by ice cold lysis buffer (150 mM NH_4Cl, 10 mM $NaHCO_3$, 1 mM EDTA) before staining. For analysis of BM in CD45.1 mice transplanted with LN cells from leukemic *Pax5*$^{+/-}$ *Ebf1*$^{+/-}$ mice, cells were

stained with antibodies against CD45.1 (A20), CD45.2 (104) and CD19 (6D5) for investigation of tumor burden and for myelo-erythroid progenitors with lineage markers CD11b/Mac1 (M1/70), Gr1 (RB6-8C5), TER119 (TER119), CD3e (145-2C11, eBioscience (eBio)), CD11c (N418) and NK1.1 (PK136) together with CD19 (6D5), CD16/32 (93), CD105 (MJ7/18), CD150 (TC15-12F12.2), KIT (2B8, BD), SCA1 (D7), and CD41 (MWReg30). CD45.1 (A20, BD) was added to the analysis in LSKCD150 transplantation models. For the more detailed HSC phenotyping, cells were stained with CD45.1 (A20, BD), SCA-1 (D7), CD48 (HM48-1, eBio), CD201 (1560, eBio), CD150 (TC15-12F12.2), KIT (2B8, BD), CD19 (6D5) and lineage antibodies (NK1.1 (PK136), CD11C (N418), CD11B (M1/70), GR1 (RB6-8C5), TER119 (TER119), CD3e (145-2C11, eBio). Antibodies are from Biolegend unless otherwise stated. Propidium iodide (PI, Invitrogen, Paisly UK) was generally used as a viability marker and gates for each indicated cell population were set according to fluorescence minus one (FMO) controls. Analysis and cell sorting were performed on a LSRFortessaX20 and AriaIII (BD Biosciences, San Jose, California).

In vitro culture of Myelo-Erythroid progenitors.

BM and spleen HSC cells from PBS or LN768 transplanted CD45.1 mice, 19 days after transplantation, were pooled (PBS or LN768, (TM)) and lineage depleted using Invitrogen Dynabeads Sheep-anti-Rat cat 11035 and purified CD19 (6D5), GR1 (RB6-8C5), CD4 (GK1.5), CD8a (53-6.7), CD11b/Mac1 (M1/70), TER119 (TER119) antibodies. Lineage depleted cells were stained with antibodies against CD45.1 (A20), SCA-1 (D7), CD150 (TC15-12F12.2), KIT (2B8), CD19 (6D5) and lineage antibodies (NK1.1 (PK136), CD11C (N418), CD11B (M1/70), GR1 (RB6-8C5), TER119 (TER119), CD3e, (145-2C11, eBio). Singlet PI^- $LSKCD45.1^+CD150^+$ cells were sorted and duplicate dishes of 50 cells and plated in Methocult M3434 media (StemCell Technologies), a commercial product containing a pre added cytokine

cocktail allowing for the development of myeloid and erythroid cells. The dishes were read at day 10 for total colony, BFU-E, CFU-GM, CFU-G, CFU-M and CFU-GEMM count.

Single cell cloning assay.

To determine the functional efficiency of progenitor cell populations in BM and spleen we harvested cells from mice with fully developed leukemia (>80% of BM cells leukemia). Spleen and BM were isolated as above. The samples were lineage depleted through incubation with biotinylated antibodies against lineage hematopoietic surface-markers CD5 (53-7.3), CD11b (M1/70), Gr-1 (RB6-8C5), CD19 (6D5), B220 (RA3-6B2), and TER119 (TER119), all BioLegend), followed by the StemCell EasySep negative selection kit as per the manufacturer's instructions. BM and spleen cell suspensions enriched for lineage negative cells were stained with antibodies against hematopoietic surface marker for 20 minutes at 4ºC. Followed by washing in 2 mL of PBS no adds and resuspending all samples in 200 µL of PBS containing 2 % FCS and 0,5 % BSA. All populations were sorted based on expression of CD45.1 (A20). Long term stem cells (LT-HSC) were sorted as live (LIVE/DEAD™ Fixable Near IR (780) Viability Kit (Thermo scientific)), Lin^-(CD4 (RM4-5), CD8a (53-6.7), CD11b (M1/70), CD11c (N418), CD19 (6D5), GR1 (RB6-8C5), NK1.1(PK136), TER119 (TER119), KIT $(2B8)^+$ SCA1 $(D7)^+$, (LSK) and $CD150^+$ (TC15-12F12) $CD201^+$ (RCR-16) $CD48^-$ (HM48-1), short term stem cells (ST-HSC) were sorted as LSK $CD48^-$ $CD150^-$, MPP (LSK $CD48^+$) using FACS (Aria III). BM and spleen cells from healthy (PBS) or leukemia (LN768) transplanted CD45.1.2 mice were sorted on a FACS Aria III.

Single progenitor cells were sorted into Methocult M3434 media (StemCell Technologies) in 96-well plates and incubated for 10 days. Wells were analyzed using light microscopy (Leica DMIL) to determine the number of colonized well. Five wells from each individual mice, cell

type, and tissue were then resuspended into individual FACS-tubes and washed using 3 mL of PBS containing 2 % FCS and 0,5 % BSA. All samples were resuspended in 100 µL of PBS containing 2 % FCS and 0,5 % BSA and stained against hematopoietic surface markers for 20 minutes at 4ºC. Followed by washing in 2 mL of PBS and resuspending all samples in 50 µL of PBS containing 2 % FCS and 0,5 % BSA before analysis on the Cytek Aurora (Cytek Biosciences). The live cells were analyzed for expression of CD71 (C2)(BD), SCA1 (C7), Ly6G (1A8), Ly6C (HK14), CD16/32 (MWReg30), KIT (2B8), CD41 (MWReg30), CD105 (MJ7/18), CD11b (M1/70), TER-119 (TER-119), CD150 (TC15-12F12) and CD45 (30-F11). Erythroid cells were identified as $CD45^{low/neg}$ $CD71^{+}$ and monocytes as $CD45^{+}$ $CD11b^{+}$ $CD16/32^{+}$ $Ly6c^{+}$. Flow cytometry data were analyzed using OMIQ (Dotmatics). Visualization and statistical modelling were performed using GraphPad Prism version 10.0.0 for Windows (GraphPad Software Inc).

Transplantation of spleen HSC

BM and spleen HSC cells from PBS or LN768 leukemia (B-ALL) transplanted CD45.1 mice, 18 days after transplantation, were pooled (PBS or LN768, (TM)) and lineage depleted using Invitrogen Dynabeads Sheep-anti-Rat cat 11035 and purified CD19 (6D5), GR1 (RB6-8C5), CD4 (GK1.5), CD8a (53-6.7), CD11b/Mac1 (M1/70), TER119 (TER119) antibodies. Lineage depleted cells were stained with antibodies against CD45.1 (A20, BD), SCA-1 (D7), CD48 (HM48-1, eBio), CD201 (1560, eBio), CD150 (TC15-12F12.2), KIT (2B8, BD), CD19 (6D5) and lineage antibodies (NK1.1 (PK136), CD11C (N418), CD11B (M1/70), GR1 (RB6-8C5), TER119 (TER119), CD3e, (145-2C11, eBio). Singlet PI^{-} LSK $CD45.1^{+}$ $CD48^{-}$ $CD150^{+}$ $CD201^{+}$ cells were sorted and 50 cells per recipient were transplanted together with 200,000 whole BM support (CD45.2) to lethally irradiated (9 Gy) C57BL/6 (CD45.2) mice. Peripheral blood (PB) lineage staining of transplanted mice was performed with antibodies against CD45.1 (A20), CD45.2 (104), GR1 (RB6-8C5), MAC1 (M1/70), CD3 (17A2), CD19 (6D5)

and myelo-erythroid progenitor engraftment was tracked with lineages markers (CD11b/Mac1 (M1/70), Gr1 (RB6-8C5), TER119 (Ter119), CD3e (145-2C11, eBio), CD11c (N418) and NK1.1 (PK136)) together with CD19 (6D5), CD16/32 (93), CD105 (MJ7/18), CD150 (TC15-12F12.2), KIT (2B8), SCA1 (D7), and CD41 (MWReg30, eBio). Mice were bled at 4, 8, 16 and 24 weeks for FACS analysis and after 24 weeks, the presence of myelo-erythroid progenitors in the BM and spleen was determined (antibodies as above). Antibodies were purchased from Biolegend unless otherwise stated.

Isolation of cells for SC-RNA seq

Stromal cells were isolated from BM and spleen from PBS or LN768 transplanted CD45.1 mice 16-19 days after transplantation. Bones and spleen were crushed and suspension cells moved to separate tubes. Cells from bone fragments and spleen husk were further isolated at 37°C for 45 minutes in HBSS media supplemented with collagenaseII (1mg/ml, Worthington Biochemical) and Dnase1 (10ug/ml, Sigma), suspension cells were collected, bone and spleen fragments washed with PBS and then treated with 0.05% Trypsin-EDTA (Gibco) for 15 minutes at 37°C. Suspension cells were pooled and lineage depleted using Invitrogen Dynabeads Sheep-anti-Rat cat 11035 and purified B220 (RA3-6B2), GR1 (RB6-8C5), CD3 (N418), CD45 (30-F11) and TER119 (TER119) antibodies. For the BM data set (Figure 3), lineage depleted cells were stained with a lineage cocktail against positive markers for stromal cells (CD51 (RMV-7), CD31 (390), CD44 (IM7), CD34 (RAM34, eBio), CD106 (429, eBio), CD114 (16B10), CD140a (APA5), SCA1 (D7)) and LepR (MA5-32685, Invitrogen) as well as CD45 (30-F11), Ter119 (TER119)), CD71 (RI7217), B220 (RA3-6B2), CD11B (M1/70) and CD19 (6D5). 6,764-15,000 PI^-Singlets $CD45^-CD19^-B220^-Ter119^-CD71^-Lin^+Lepr^+$ cells were sorted for single cell RNA sequencing. For the spleen data set (Figure 2), CD71 (RI7217), CD45.1 (A20, BD), CD45.2 (A20), CD19 (6D5) lineage antibodies (CD45 (30-F11), Ter119

(Ter119)), B220 (RA3-6B2), CD11B (M1/70) and CD3e (145-2C11, eBio), CD11c (N418) and NK1.1 (PK136)). 5,588 to 6917 singlet Lin^- $CD45^-$ $CD45.1^-$ PI^- cells were sorted for single cell RNA sequencing.

Single cell RNA Sequencing and data analysis.

Libraries were prepared and sequenced at Center for Translational Genomics (CTG) at Lund university using the 10x Genomics Chromium platform with the Single-cell Gene Expression (3´GEX) library preparation (v3.1, sc mRNAseq).

Fastq files and gene count matrices were generated using *Cell Ranger* v4. The resulting count tables from each condition were processed using *Scanpy* v1.10.1. Mitochondrial and ribosomal genes (matching the regular expressions `'^[Mm][Tt]-'` and `'^R[pP][SsLl]'`, respectively) were removed prior to normalization. Cells with more than 1,000 detected UMIs and expression for at least 100 genes were retained and normalized by down-sampling to 1,000 UMIs per cell. The 300 most variable genes were selected for PCA and UMAP computation. *Leiden* clusters were identified using default parameters, and differentially expressed genes were determined with the `rank_genes_groups` function. Functions for generating dot plots, bar graphs, and heatmaps are available at: https://github.com/stela2502/ScanpyAutoAnalyzer.

Analysis notebooks and scripts used to process data and generate several of the plots of scRNA seq data shown in Figures 2 and 3 are accessible at: https://github.com/stela2502/BMResilience_ScRNAseq. In the note book, “experiment 3” refers to data in figure 2 and “experiment 2” data in figure 3.

Immunofluorescent staining and histology.

Leukemic and control spleens were fixed in periodate-lysine-paraformaldehyde solution and cryo protected in sucrose solution before embedded in optimal cutting temperature (OCT) compound (Ref# LAMB/OCT) on dry ice, and stored at -80 °C.

Tissue sections with 10 µm thickness were washed in PBS for tissue rehydration and the OCT compound removal and blocked with 2% fetal bovine serum (FBS) + 1% bovine serum albumin. The sections were covered with 150-200 µl antibody cocktails in PBS at 4 °C overnight. Anti-CD45.2 (biotin anti-mouse CD45.2 (clone 104) BioLegend, 1:400) was used to stain the tumor cells, for LT-HSCs staining we used anti-EPCR/CD201 (biotin anti-mouse CD201 (EPCR) and anti-CD48 antibody. Anti-CD31 antibody (Alexa Fluor® 647) was used to visualize the endothelial cells (ECs). The nuclei were stained by DAPI. The samples were imaged using Leica DMi8 inverted widefield microscope (Wetzlar, Germany) and LASX software (Leica Microsystems). To count the EPCR/CD201$^+$ CD48$^-$ cells, 20 random fields of view of the leukemic spleens and 15 random fields of view of the control spleens were selected. The distance between the HSCs' membrane and the nearest ECs observed in the same fields of view was measured by Fiji (ImageJ 1.54d) software. To quantify the relative presence of endothelia cells CD31$^+$ area and the whole image area of 9 images of the leukemic spleens and 9 images of the control spleens were measured by Fiji (ImageJ 1.54p) and the percent of CD31$^+$ area in each image was calculated. GraphPad Prism 10 was used to analyze the quantitative data, obtained by Fiji. Student's t-tests were applied, and P values smaller than 0.05 was considered significant.

ELISA from bone marrow and spleen samples.

Spleen tissues were forced through a nylon mesh, 100 µL of PBS were added to the mesh followed by centrifugation. BM samples was isolated from the tibia bones of each mouse. The edges of the tibia were removed with scissors and flushed with 100 µL of PBS. The cell suspension was then collected in an Eppendorf tube, before being centrifugation and the concentration of CXCL12 in the supernatant was deterined using the Mouse SDF-1 Alpha CXCL12 ELISA Kit.

In vivo leukemia depletion (Killswitch) experiments.

CRISPR guides that induced cell death were identified by looking for guides with a low specificity score in a repetitive area of the genome using Benchling (Biology Software. 2020). Chosen guides (sg292; GGAGCACTGTGACACCACAG and sg294; GGAGTACTGTGACACCACAG or sgR26 control; GCCGGTGCGCCGCCAATCAG) were cloned into pAW13.lentiGuide-emCherry plasmid (lentiguide-mCherry, Addgene plasmid # 104375) and pAW12.lentiGuide-eGFP plasmid (Addgene#: 104374, gifts from Richard Young). Lentiviruses were produced and used to infect leukemic LN cells. Cells were expanded in vitro and sorted as $CD45^+$ $mCherry^+$ GFP^+ $CD19^+$ Killswitch (KS) or $CD45^+$ $mCherry^{+m}CD19^+$ (R26) before transplantation of 150,000 cells/recipient were into $CD45.1^+$ iCas9/C57BL/6 non-conditioned animals. At 14 day post transplantation, recipient mice were either treated with doxycycline (one i.p. injection 2 mg/mouse (Sigma) as well as Dox chow, Dox high pellets 2g/kg, (ssniff Spezialdiäten, Germany)) to induce Cas9 expression or analyzed as day0. Induced mice were then analyzed at day 4, 8 and 14 post induction with Dox.

Reanalysis of patient BM samples

Patient BM B-ALL samples (median age 6.5, 0-59 years) from diagnosis and 15-, 29- or 78-79-days post start of treatment according to the NOPHO2008 protocol (3), was compared to BM from healthy donor or lymphoma patients without BM engagement (4). Samples were stained for expression of CD66c, CD58, CD20, CD38, CD19, CD123, CD34, CD10, CD22, and CD45 before analysis through flow cytometry on the Navios flow cytometer (Beckman Coulter) as described in (4). The data were reanalyzed with consent from the Swedish National ethics board.

UMAP for the visualization of BM recovery was generated based on the expression of all stained for surface markers and FlowSOM clustering was then used to create an unbiased visualization of population distribution. Clusters were recognized as either linage negative ($CD45^+$, $CD34^+$, $CD19^-$, $CD20^-$, $CD22^-$, $CD66c^-$), erythroid linage ($CD10^-$, $CD19^-$, $CD20^-$, $CD22^-$, $CD45^-$, $CD66c^-$), myeloid linage ($CD45^+$, $CD19^-$, $CD20^-$, $CD22^-$, together with the expression of CD38 and/or CD66c), lymphoid linage ($CD45^+$, $CD66c^-$, together with the expression of either CD10, CD19, CD20, or CD22), or $CD19^+$ B-ALL (all $CD19^+$ cell clusters present in leukemia samples but missing in control samples). Linage negative cells were also further divided into early and late progenitors based on their expression of CD38, a protein not expressed on HSCs.

Flow cytometry data were analyzed and visualized using OMIQ (Dotmatics). All statistical modelling was performed using GraphPad Prism version 10.0.0 for Windows (GraphPad Software Inc). Statistical significance is compared between control and patient samples, * $P < 0.05$, ** $P < 0.01$, *** $P < 0.001$, **** $P < 0.0001$.

References:

1. Prasad MA, Ungerback J, Ahsberg J, Somasundaram R, Strid T, Larsson M, Mansson R, De Paepe A, Lilljebjorn H, Fioretos T, Hagman J, Sigvardsson M. Ebf1 heterozygosity results in increased DNA damage in pro-B cells and their synergistic transformation by Pax5 haploinsufficiency. Blood. 2015 Jun 25;125(26):4052-9. doi:10.1182/blood-2014-12-617282. Cited in: Pubmed; PMID 25838350.

2. Van den Broeck W, Derore A, Simoens P. Anatomy and nomenclature of murine lymph nodes: Descriptive study and nomenclatory standardization in BALB/cAnNCrl mice. J Immunol Methods. 2006 May 30;312(1-2):12-9. Epub 2006/04/21. doi:10.1016/j.jim.2006.01.022. Cited in: Pubmed; PMID 16624319.

3. Toft N, Birgens H, Abrahamsson J, Griskevicius L, Hallbook H, Heyman M, Klausen TW, Jonsson OG, Palk K, Pruunsild K, Quist-Paulsen P, Vaitkeviciene G, Vettenranta K, Asberg A, Frandsen TL, Marquart HV, Madsen HO, Noren-Nystrom U, Schmiegelow K. Results of NOPHO ALL2008 treatment for patients aged 1-45 years with acute lymphoblastic leukemia. Leukemia. 2018 Mar;32(3):606-615. Epub 2017/08/19. doi:10.1038/leu.2017.265. Cited in: Pubmed; PMID 28819280.

4. Modvig S, Hallbook H, Madsen HO, Siitonen S, Rosthoj S, Tierens A, Juvonen V, Osnes LTN, Valerhaugen H, Hultdin M, Matuzeviciene R, Stoskus M, Marincevic M, Lilleorg A, Ehinger M, Noren-Nystrom U, Toft N, Taskinen M, Jonsson OG, Pruunsild K, Vaitkeviciene G, Vettenranta K, Lund B, Abrahamsson J, Porwit A, Schmiegelow K, Marquart HV. Value of flow cytometry for MRD-based relapse prediction in B-cell precursor ALL in a multicenter setting. Leukemia. 2021 Jul;35(7):1894-1906. Epub 2020/12/16. doi:10.1038/s41375-020-01100-5. Cited in: Pubmed; PMID 33318611.

Progenitor Population	**Markers**	**Comments**
LSK cells	Lineage^{-} (Lin^{-}) SCA1^{High} KIT^{High}	Lineage markers CD19, NK1.1 CD11C, CD11B, GR1, TER119 CD3e
LSKCD150+	LSK CD150^{+}	Figure 1C, 2D, S1E, 7C, 7D
LSKCD150-	LSK CD150^{-}	Figure 1C, 2D, 7C
Long term (LT) HSC	LSK CD150^{+} CD201^{+} CD48^{-}	Figure 1E, 2B, C, S1D
Short term (ST) HSC	LSK CD150^{-} CD48^{-}	Figure 1E, 2B, S1D
Multipotent progenitor (MPP) 2	LSK CD150^{+} CD48^{+}	Figure 1E, 2B, S1D
MPP 3-4	LSK CD150^{-} CD48^{+}	Figure 1E, 2B, S1D
MkP	Lin^{-} SCA1^{-} KIT^{High} (LK) CD150^{+} CD41^{+}	Figure 1C, 2D, 7C
GMP	LK CD41^{-} CD16/32^{+}	Figure 1C, 2D, 7C
pGM	LK CD41^{-} CD16/32^{-} CD105^{-} CD150^{-}	Figure 1C, 2D, 7C
PmegE	LK CD41^{-} CD16/32^{-} CD105^{-} CD150^{+}	Figure 1C, 2D, 7C
CFU-E	LK CD41^{-} CD16/32^{-} CD105^{+} CD150^{-}	Figure 1C, 2D, 7C
pCFU-E	LK CD41^{-} CD16/32^{-} CD105^{+} CD150^{+}	Figure 1C, 2D, 7C

Table S1: Markers used for the definition of progenitor populations.